Inorganic Chemistry

Article

pubs.acs.org/IC

# Isostructural Dinuclear Phenoxo-/Acetato-Bridged Manganese(II), Cobalt(II), and Zinc(II) Complexes with Labile Sites: Kinetics of Transesterification of 2-Hydroxypropyl-*p*-nitrophenylphosphate

Himanshu Arora,[†] Suman K. Barman,[†] Francesc Lloret,[‡] and Rabindranath Mukherjee*[,†,§]

[†]Department of Chemistry, Indian Institute of Technology Kanpur, Kanpur 208 016, India

[‡]Departament de Química Inorgànica/Instituto de Ciencia Molecular (ICMOL), Universitat de València, Polígono de la Coma, s/n, 46980-Paterna (València), Spain

Supporting Information

**ABSTRACT:** Using the dinucleating phenol-based ligand 2,6-bis[3-(pyridin-2-yl)pyrazol-1-ylmethyl]-4-methylphenol] ($HL^2$), in its deprotonated form, the six new dinuclear complexes $[M^{II}_2(L^2)(\mu\text{-}O_2CMe)_2(MeCN)_2][PF_6]$ (M = Mn (**2a**), Co (**3a**), Zn (**4a**)) and $[M^{II}_2(L^2)(\mu\text{-}O_2CMe)_2(MeCN)_2][BPh_4]$ (M = Mn (**2b**), Co (**3b**), Zn (**4b**)) have been synthesized. Crystallographic analyses on **2b**·2MeCN, **3b**·2MeCN, and **4b**·2MeCN reveal that these complexes have closely similar $\mu$-phenoxo bis($\mu$-carboxylato) structures. The physicochemical properties (absorption and ESI-MS spectral data, **2a**,**b**, **3a**,**b**, and **4a**,**b**; $^1$H NMR, **4a**,**b**) of the cations of **2a**−**4a** are identical with those of **2b**−**4b**. Each metal ion is terminally coordinated by a pyrazole nitrogen and a pyridyl nitrogen from a 3-(pyridin-2-yl)pyrazole unit and a solvent molecule (MeCN). Thus, each metal center assumes distorted-octahedral $M^{II}N_3O_3$ coordination. Temperature-dependent magnetic studies on $Mn^{II}$ and $Co^{II}$ dimers reveal the presence of intramolecular antiferromagnetic ($J$ = −8.5 cm$^{-1}$) for **2b** and ferromagnetic exchange coupling ($J$ = +2.51 cm$^{-1}$) for **3b**, on the basis of the Hamiltonian $H = -JS_1 \cdot S_2$. The exchange mechanism is discussed on the basis of magneto-structural parameters (M···M distance). Spectroscopic properties of the complexes have also been investigated. The pH titration and kinetics of phosphatase (transesterification) activity on 2-hydroxypropyl-*p*-nirophenylphosphate (HPNP) were studied in MeOH/$H_2O$ (33%, v/v) with **2a**−**4a**, due to solubility reasons. This comparative kinetic study revealed the effect of the metal ion on the rate of hydrolysis of HPNP, which has been compared with what we recently reported for $[Ni^{II}_2(L^2)(\mu\text{-}O_2CMe)_2(MeOH)(H_2O)][ClO_4]$ (**1a**). The efficacy in the order of conversion of substrate to product (*p*-nitrophenolate ion) follows the order **4a** > **3a** > **2a** > **1a**, under identical experimental conditions. Notably, this trend follows the decrease of p$K_a$ values of $M^{II}$-coordinated water (7.95 ± 0.04 and 8.78 ± 0.03 for **1a**, 7.67 ± 0.08 and 8.69 ± 0.06 for **2a**, 7.09 ± 0.05 and 8.05 ± 0.06 for **3a**, and 6.20 ± 0.04 and 6.80 ± 0.03 for **4a**). In this work we demonstrate that the stronger the Lewis acidity ($Z_{eff}/r$) of the metal ion, the more acidic is the $M^{II}$-coordinated water and the greater is the propensity of the metal ion to catalyze hydrolysis of the activated phosphate ester HPNP. Notably, the observed $k_2$ values ($M^{-1}$ s$^{-1}$) for $Mn^{II}$ (**2a**, 0.152), $Co^{II}$ (**3a**, 0.208), and $Zn^{II}$ (**4a**, 0.230) complexes (**1a**, 0.058; already reported) linearly correlate with $Z_{eff}/r$ values of the metal ion. In each case a pseudo-first-order kinetic treatment has been done. Kinetic data analysis of complexes **2a**−**4a** were also done following Michaelis−Menten treatment (catalytic efficiency $k_{cat}/K_M$ values 0.170 $M^{-1}$ s$^{-1}$ for **2a**, 0.194 $M^{-1}$ s$^{-1}$ for **3a** and 0.161 $M^{-1}$ s$^{-1}$ for **4a**; for **1a** the value is 0.089 $M^{-1}$ s$^{-1}$). Temperature-dependent measurements were done to evaluate kinetic/thermodynamic parameters for the hydrolysis/transesterification of HPNP and yielded comparable activation parameters ($E_a$ (kJ mol$^{-1}$): 71.00 ± 4.60 (**1a**; reported), 67.95 ± 5.71 (**2a**), 62.60 ± 4.46 (**3a**), 67.80 ± 3.25 (**4a**)) and enthalpy/entropy of activation values ($\Delta H^{\ddagger}$ (kJ mol$^{-1}$) = 68.00 ± 4.65 (**1a**; reported), 65.40 ± 5.72 (**2a**), 60.00 ± 4.47 (**3a**), 65.29 ± 3.26 (**4a**); $\Delta S^{\ddagger}$ (J mol$^{-1}$ K$^{-1}$) = −109.00 ± 13 (**1a**; reported), −107.30 ± 16 (**2a**), −122.54 ± 14 (**3a**), −104.67 ± 10 (**4a**)). The $E_a$ values for all the complexes are comparable, suggesting a closely similar reaction barrier, meaning thereby similar course of reaction. The $\Delta S^{\ddagger}$ values are consistent with an associative process. Positive $\Delta H^{\ddagger}$ values correspond to bond breaking of the activated complex as a result of nucleophilic attack at the phosphorus atom, releasing cyclic phosphate and *p*-nitrophenolate ion. These data have helped us to propose a common mechanistic pathway: deprotonation of a metal-bound species to form the effective nucleophile, binding of the substrate to the metal center(s), intramolecular nucleophilic attack on the electrophilic phosphorus atom with the release of the leaving group, and possibly regeneration of the catalyst.

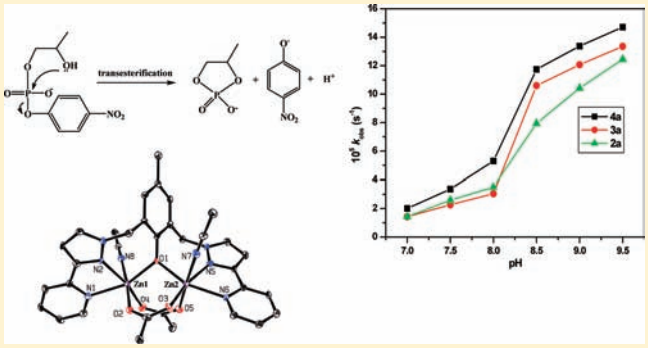


**Received:** September 7, 2011
**Published:** April 26, 2012

## INTRODUCTION

Bimetallic cores exist at active sites of many enzymes and play an essential role in biological systems. The present work derives impetus from the active sites of metallohydrolases.[1,2] Binuclear metallophosphatases are important in an array of biochemical processes involving the hydrolysis of phosphate ester bonds. To understand the biological significance of such bimetallic cores and the functions of binuclear metallohydrolases in general and binuclear metallophosphatases in particular at the molecular level, studies with suitable bioinspired models remain increasingly important.[3−18] In this context the effect of metal−ligand bonding interactions to modulate the acidity of $M^{II}-H_2O$ to generate the active form $M^{II}-OH$, which will act as a nucleophile for the hydrolysis reactions, is of utmost significance.[19] Ideally, the $pK_a$ value for such a process should be closer to optimal physiological conditions (pH ∼7.4). From this perspective we directed our focus toward the synthesis of a (solv)$M^{II}$−($\mu$-phenoxo)−$M^{II}$(solv) dinuclear unit (solv = solvent), supported terminally by bidentate (2-pyridyl)alkylamine ($(L^1)^-$) or 3-(2-pyridyl)pyrazole unit ($(L^2)^-$) (Chart 1) and additionally

**Chart 1. Structures of the Ligands**

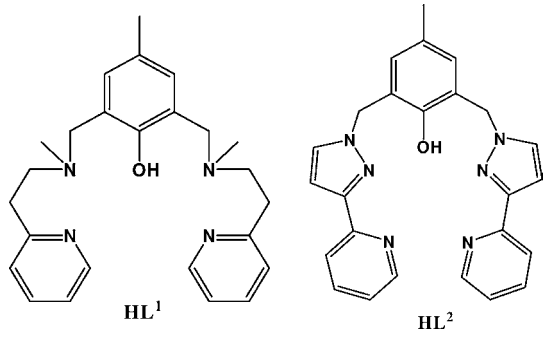


supported either by terminally coordinated chelating carboxylate or by bis-$\mu_{1,3}$-carboxylate (*syn-syn* conformation) bridges.[20] As a first step toward this goal we recently reported the synthesis of $[Ni^{II}_2(L^1)(O_2CMe)_2(H_2O)_2][PF_6]\cdot MeOH\cdot 3H_2O$, $[Ni^{II}_2(L^2)(\mu\text{-}O_2CMe)_2(MeOH)(H_2O)][ClO_4]$ (**1a**), and $[Ni^{II}_2(L^2)(\mu\text{-}O_2CMe)_2(MeOH)(H_2O)][BPh_4]\cdot 3MeOH\cdot H_2O$ (**1b**), having labile coordination sites (water/methanol) to generate $Ni^{II}$-bound hydroxide ions as nucleophiles, and investigated the potential of the complexes $[Ni^{II}_2(L^1)(O_2CMe)_2(H_2O)_2][PF_6]\cdot MeOH\cdot 3H_2O$ and **1a** (while $[Ni^{II}_2(L^1)(O_2CMe)_2(H_2O)_2][PF_6]\cdot MeOH\cdot 3H_2O$ and **1b** were structurally characterized, the pH titration and transesterification experiments were done on $[Ni^{II}_2(L^1)(O_2CMe)_2(H_2O)_2][PF_6]\cdot MeOH\cdot 3H_2O$ and **1a**, due to their solubility in MeOH/$H_2O$ medium (33%, v/v)) toward hydrolysis/transesterification of an activated phosphoric acid ester, 2-hydroxypropyl-*p*-nitrophenylphosphate (HPNP).[20] Our studies reinforced the notion that as the $Ni^{II}$−ligand interaction becomes weak, the $Ni^{II}-H_2O$ bond becomes strong, resulting in the ease of deprotonation of coordinated water. The complex $[Ni^{II}_2(L^1)(O_2CMe)_2(H_2O)_2][PF_6]\cdot MeOH\cdot 3H_2O$ showed a higher rate of HPNP hydrolysis in comparison to complex **1a**.

Attempts have been made to pinpoint the effect of the Lewis acidity of the metal ion,[6,14−19] either by keeping the metal ion fixed and varying the ligand systems and/or keeping the ligand system invariant and changing the metal ion, toward hydrolysis of phosphate esters in general and hydrolysis of HPNP in particular. The catalysis of the hydrolysis of phosphate triesters and both phosphodiesters and phosphotriesters by $Zn^{II}$ complexes was investigated, and an inverse correlation between the activity of the $Zn^{II}$ complexes and the $pK_a$ value of $Zn^{II}-H_2O$ was observed.[17a,b] However, opposite effects, i.e. an increase in the catalytic activity of the $Cu^{II}$ complexes for phosphodiester and phosphotriester hydrolysis with increasing $pK_a$ value of $Cu^{II}-H_2O$[17c] and a positive correlation of the reaction rate of the phosphate diester hydrolysis of the $Zn^{II}$ complexes[18] and the basicity of $Zn^{II}-H_2O$, have also been observed.[5a] The latter correlations indicate that the efficiency of the nucleophile determines the intrinsic reactivity of the $Cu^{II}/Zn^{II}$ complexes. Although metal-mediated phosphate ester hydrolysis has been studied for several decades, clearly further investigations are needed. This background sets the stage for the present investigation. The primary focus of this work is to investigate the effect of bivalent metal ions on the rate of hydrolysis of HPNP for isostructural $\mu$-phenoxo-bis($\mu_2$-1,3-acetato) dimetal(II) complexes, with a labile coordination site at each metal center, of high-spin $Mn^{II}$ ($d^5$ system), high-spin $Co^{II}$ ($d^7$ system), and of the $Zn^{II}$ ion ($d^{10}$ system), supported by an invariant dinucleating ligand ($(L^2)^-$). We present herein a comprehensive report on the synthesis and properties of $[Mn^{II}_2(L^2)(\mu\text{-}O_2CMe)_2(MeCN)_2]X$ (X = $PF_6^-$/$BPh_4^-$, **2a**,**b**), $[Co^{II}_2(L^2)(\mu\text{-}O_2CMe)_2(MeCN)_2]X$ (X = $PF_6^-$/$BPh_4^-$, **3a**,**b**), and $[Zn^{II}_2(L^2)(\mu\text{-}O_2CMe)_2(MeCN)_2]X$ (X = $PF_6^-$/$BPh_4^-$, **4a**,**b**). The molecular structures of **2b**·2MeCN, **3b**·2MeCN, and **4b**·2MeCN have been elucidated. The magnetic properties of $[Mn^{II}_2(L^2)(\mu\text{-}O_2CMe)_2(MeCN)_2][BPh_4]$ (**2b**) and $[Co^{II}_2(L^2)(\mu\text{-}O_2CMe)_2(MeCN)_2][BPh_4]$ (**3b**) have been investigated. Because of the presence of coordinated solvent molecules and reasonable solubility in MeOH/$H_2O$ (33%, v/v) medium, complexes **2a**−**4a** were tested for their potential to act as model catalysts in the hydrolysis of HPNP. An attempt has been made to rationalize the observed trend of the rate of hydolysis by $Mn^{II}$, $Co^{II}$, and $Zn^{II}$, and the results have been compared with those of **1a**.

## EXPERIMENTAL SECTION

**General Procedure.** All reagents and solvents were obtained from commercial sources and used as received. Solvents were dried/purified as reported previously.[20] The synthesis of 3-(2-pyridyl)pyrazole was achieved following a reported procedure.[21] The ligand $HL^2$ was synthesized as before.[20] The barium salt of 2-hydroxypropyl-*p*-nitrophenylphosphate (HPNP) was prepared following a literature procedure.[22]

**Synthesis of $[Mn^{II}_2(L^2)(\mu\text{-}O_2CMe)_2(MeCN)_2][PF_6]$ (2a).** To a solution of $HL^2$ (0.200 g, 0.47 mmol) in MeOH (10 mL) was added solid $Mn^{II}(O_2CMe)_2\cdot 4H_2O$ (0.231 g, 0.94 mmol). The resulting intensely yellow solution was stirred for 1 h at room temperature. Then $NH_4PF_6$ (0.080 g, 0.47 mmol) was added to the above solution. Addition of $Et_2O$ resulted in the precipitation of a solid, which was filtered, washed with MeOH/$Et_2O$ (1/3, v/v) mixture, and dried in vacuo. Yield: 0.160 g (40%, based on $HL^2$). Anal. Calcd for $C_{33}H_{33}F_6Mn_2N_8O_5P$ ($M_r$ = 876): C, 45.20; H, 3.77; N, 12.79. Found: C, 44.76; H, 3.44; N, 12.92. Conductivity (MeCN, 1 mM solution at 298 K): $\Lambda_M$ = 130 $\Omega^{-1}$ cm$^2$ mol$^{-1}$ (expected range[23] for 1:1 electrolyte: 120−160 $\Omega^{-1}$ cm$^2$ mol$^{-1}$). IR (KBr, cm$^{-1}$, selected peaks): 1607 ($\nu_{asym}$(CO)), 1476 ($\nu_{sym}$(CO)), 844 ($\nu(PF_6^-)$). Absorption spectrum ($\lambda_{max}$, nm ($\varepsilon$, M$^{-1}$ cm$^{-1}$); in MeCN): 245 (49 500), 290 (34 000).

**Synthesis of $[Mn^{II}_2(L^2)(\mu\text{-}O_2CMe)_2(MeCN)_2][BPh_4]$ (2b).** To a solution of $HL^2$ (0.200 g, 0.47 mmol) in MeOH (10 mL) was added solid $Mn^{II}(O_2CMe)_2\cdot 4H_2O$ (0.230 g, 0.94 mmol). The resulting intensely yellow solution was stirred for 15 min at room temperature. Then $NaBPh_4$ (0.160 g, 0.47 mmol) was added to the above solution. The pale yellow solid that precipitated was filtered, washed with a MeCN/$Et_2O$ mixture (1/3, v/v), and dried in vacuo. Single crystals of composition **2b**·2MeCN suitable for structural studies were obtained by recrystallization of the complex in 1/1 (v/v) mixture of MeCN


dx.doi.org/10.1021/ic201971t | Inorg. Chem. 2012, 51, 5539−5553

and MeOH. Yield: 0.250 g (50%, based on $HL^2$). Anal. Calcd for $C_{61}H_{59}B_1Mn_2N_{10}O_5$ ($M_r$ = 1132.87): C, 64.61; H, 5.20; N, 12.35. Found: C, 64.76; H, 5.44; N, 12.12. Conductivity (MeCN, 1 mM solution at 298 K): $\Lambda_M$ = 110 $\Omega^{-1}$ cm$^2$ mol$^{-1}$. IR (KBr, cm$^{-1}$, selected peaks): 1599 ($\nu_{asym}$(CO)), 1475 ($\nu_{sym}$(CO)), 706 ($\nu(BPh_4^-)$). Absorption spectrum ($\lambda_{max}$, nm ($\varepsilon$, M$^{-1}$ cm$^{-1}$); in MeCN): 245 (49 000), 290 (34 300).

**Synthesis of $[Co^{II}_2(L^2)(\mu\text{-}O_2CMe)_2(MeCN)_2][PF_6]$ (3a).** To a solution of $HL^2$ (0.200 g, 0.47 mmol) in MeOH (10 mL) was added solid $Co^{II}(O_2CMe)_2{\cdot}4H_2O$ (0.265 g, 0.94 mmol). The resulting reddish pink mixture was refluxed for 2 h. Then $KPF_6$ (0.086 g, 0.47 mmol) was added to the above solution. Addition of $Et_2O$ resulted in the precipitation of a solid, which was filtered, washed with MeOH/$Et_2O$ (1/3, v/v) mixture, and dried in vacuo. It was recrystallized from MeCN/$Et_2O$. Yield: 0.200 g (47%, based on $HL^2$). Anal. Calcd for $C_{33}H_{33}Co_2F_6N_8O_5P$ ($M_r$ = 1140.85): C, 44.81; H, 3.76; N, 12.67. Found: C, 44.31; H, 3.43; N, 12.39. Conductivity (MeCN, 1 mM solution at 298 K): $\Lambda_M$ = 136 $\Omega^{-1}$ cm$^2$ mol$^{-1}$. IR (KBr, cm$^{-1}$, selected peaks): 1610 ($\nu_{asym}$(CO)), 1434 ($\nu_{sym}$(CO)), 842 ($\nu(PF_6^-)$). Absorption spectrum ($\lambda_{max}$, nm ($\varepsilon$, M$^{-1}$ cm$^{-1}$); in MeCN): 241 (sh, 36 600), 287 (15 000), 470 (120), 510 (125).

**Synthesis of $[Co^{II}_2(L^2)(\mu\text{-}O_2CMe)_2(MeCN)_2][BPh_4]$ (3b).** To a solution of $HL^2$ (0.200 g, 0.47 mmol) in MeOH (10 mL) was added solid $Co^{II}(O_2CMe)_2{\cdot}4H_2O$ (0.265 g, 0.94 mmol). The resulting reddish pink mixture was refluxed for 2 h. Then $NaBPh_4$ was added to the above solution. The pink solid that precipitated was filtered, washed with a MeCN/$Et_2O$ mixture (1/3, v/v), and dried in vacuo. Single crystals of composition **3b**·2MeCN suitable for structural studies were obtained by recrystallization of the complex in a MeCN/MeOH (1/1 (v/v)) mixture. Yield: 0.220 g (40%, based on $HL^2$). Anal. Calcd for $C_{61}H_{59}BCo_2N_{10}O_5$ ($M_r$ = 1140.85): C, 64.16; H, 5.17; N, 12.27. Found: C, 63.91; H, 5.01; N, 12.39. Conductivity (MeCN, 1 mM solution at 298 K): $\Lambda_M$ = 120 $\Omega^{-1}$ cm$^2$ mol$^{-1}$. IR (KBr, cm$^{-1}$, selected peaks): 1605 ($\nu_{asym}$(CO)), 1435 ($\nu_{sym}$(CO)), 705 ($\nu(BPh_4^-)$). Absorption spectrum ($\lambda_{max}$, nm ($\varepsilon$, M$^{-1}$ cm$^{-1}$); in MeCN): 241 (sh, 36 100), 287 (15 200), 470 (135), 510 (140).

**Synthesis of $[Zn^{II}_2(L^2)(\mu\text{-}O_2CMe)_2(MeCN)_2][PF_6]$ (4a).** To a solution of $HL^2$ (0.200 g, 0.47 mmol) in MeOH (10 mL) was added solid $Zn^{II}(O_2CMe)_2{\cdot}2H_2O$ (0.206 g, 0.94 mmol). The resulting yellow mixture was stirred for 1 h. Then $KPF_6$ (0.086 g, 0.47 mmol) was added to the above solution. Addition of $Et_2O$ resulted in the precipitation of a solid, which was filtered, washed with an MeOH/diethyl ether (1/3, v/v) mixture, and dried in vacuo. It was recrystallized from MeCN/$Et_2O$. Yield: 0.270 g (63%, based on $HL^2$). Anal. Calcd for $C_{33}H_{33}Co_2F_6N_8O_5P$ ($M_r$ = 1153.8): C, 44.17; H, 3.71; N, 12.49. Found: C, 44.66; H, 3.54; N, 12.25. Conductivity (MeCN, 1 mM solution at 298 K): $\Lambda_M$ = 130 $\Omega^{-1}$ cm$^2$ mol$^{-1}$. IR (KBr, cm$^{-1}$, selected peaks): 1609 ($\nu_{asym}$(CO)), 1439 ($\nu_{sym}$(CO)), 840 ($\nu(PF_6^-)$). $^1$H NMR (400 MHz, $CDCl_3$): $\delta$ 8.893 ($J_{H-H}$ = 5.2 Hz, 2H, d, pyridine H$^6$), 8.094 ($J_{H-H}$ = 6.4 Hz, 2H, t, pyridine H$^4$), 7.952 (1H, m, pyridine H$^5$), 7.905 ($J_{H-H}$ = 7.8 Hz, 2H, d, pyridine H$^3$), 7.60 ($J_{H-H}$ = 5.36 Hz, 2H, d, pyrazole H$^3$), 7.15 (2H, s, aromatic H$^{3,5}$), 6.89 ($J_{H-H}$ = 2.20 Hz, 2H, d, pyrazole H$^4$), 5.678 ($J_{H-H}$ = 13.44, 2H, d, $-CH_2N_3C_8H_6$), 4.947 ($J_{H-H}$ = 13.44 Hz, 2H, d, $-CH_2N_3C_8H_6$), 2.16 (15H, s, $-CH_3C_6H_2$, $-CH_3CO_2$, $CH_3CN$).

**Synthesis of $[Zn^{II}_2(L)(\mu\text{-}O_2CMe)_2(MeCN)_2][BPh_4]$ (4b).** To a solution of $HL^2$ (0.200 g, 0.47 mmol) in MeOH (10 mL) was added solid $Zn^{II}(O_2CMe)_2{\cdot}2H_2O$ (0.206 g, 0.94 mmol). The resulting yellow mixture was stirred for 1 h. Then $NaBPh_4$ was added to the above solution. The yellow solid that precipitated was filtered, washed with a MeCN/$Et_2O$ mixture (1/3, v/v), and dried in vacuo. Single crystals of composition **4b**·2MeCN suitable for structural studies were obtained by recrystallization of the complex in a MeCN/MeOH (1/1 (v/v)) mixture. Yield: 0.270 g (50%, based on $HL^2$). Anal. Calcd for $C_{61}H_{59}BN_{10}O_5Zn_2$ ($M_r$ = 1153.8): C, 63.44; H, 5.11; N, 12.14. Found: C, 63.76; H, 5.14; N, 12.39. Conductivity (MeCN, 1 mM solution at 298 K): $\Lambda_M$ = 120 $\Omega^{-1}$ cm$^2$ mol$^{-1}$. IR (KBr, cm$^{-1}$, selected peaks): 1605 ($\nu_{asym}$(CO)), 1435 ($\nu_{sym}$(CO)), 705 ($\nu(BPh_4^-)$). $^1$H NMR (400 MHz, $CDCl_3$; Figure S1, Supporting Information): $\delta$ 8.845 ($J_{H-H}$ = 5 Hz, 2H, d, pyridine H$^6$), 7.852 ($J_{H-H}$ = 7.7 Hz, 2H, t, pyridine H$^4$), 7.540 ($J_{H-H}$ = 7.8 Hz, 2H, d, pyridine H$^3$), 7.479–7.415 (6H, m, pyridine H$^5$, aromatic H$^{10}$), 7.253 (8H, s, aromatic H$^9$), 7.035–6.998 (8H, m, aromatic H$^8$), 6.891 ($J_{H-H}$ = 13.6 Hz, 2H, d, pyrazole H$^3$), 6.847 (2H, s, aromatic H$^{3,5}$), 6.448 ($J_{H-H}$ = 2.2 Hz, 2H, d, pyrazole H$^4$), 5.485 ($J_{H-H}$ = 13.6 Hz, 2H, d, $-CH_2N_3C_8H_6$), 4.438 ($J_{H-H}$ = 13.6 Hz, 2H, d, $-CH_2N_3C_8H_6$), 2.150 (15H, s, $-CH_3C_6H_2$, $-CH_3CO_2$, $CH_3CN$).

**Physical Measurements.** Elemental analyses were obtained using a Thermo Quest EA 1110 CHNS-O instrument. Conductivity measurements were done with an Elico type CM-82T conductivity bridge (Hyderabad, India). Spectroscopic measurements were made using the following instruments: IR (KBr, 4000–600 cm$^{-1}$), Bruker Vector 22; electronic, Agilent 8453 diode-array spectrophotometer; ESI-MS: Waters-HAB213 spectrometer (the isotopic distribution pattern was modeled using *Molecular Weight Calculator*, version 6.45, by M. Monroe). $^1$H NMR spectra ($CDCl_3$ solution) were obtained on a Bruker WP-80 (80 MHz) spectrometer. Chemical shifts are reported in ppm referenced to TMS. $^{31}$P NMR spectra (MeOH/$H_2O$ solution, 33% v/v) were recorded on a JEOL JNM LA 500 (500 MHz) spectrometer. Chemical shifts are reported with respect to 85% $H_3PO_4$ as the external standard.

Variable-temperature magnetic susceptibility measurements on polycrystalline samples of **1b** and **2b** were performed with a Quantum Design (Model MPMSXL-5) SQUID magnetic susceptometer at València, Spain. Solution-state magnetic susceptibilities were obtained by the NMR technique of Evans[24] in MeCN with a JEOL JNM LA 400 (400 MHz) spectrometer and made use of the paramagnetic shift of the methyl protons of MeCN as the measured NMR parameter.

**Single-Crystal Structure Determination.** Single crystals of suitable dimensions were used for data collection. Diffraction intensities were collected on a Bruker SMART APEX CCD diffractometer, with graphite-monochromated Mo K$\alpha$ ($\lambda$ = 0.710 73 Å) radiation at 100(2) K. The data were corrected for absorption. The structures were solved by SIR-97, expanded by difference Fourier syntheses, and refined with the SHELXL-97 package incorporated in the WinGX 1.64 crystallographic package.[25] The positions of the hydrogen atoms were calculated by assuming ideal geometries but not refined. All non-hydrogen atoms were refined with anisotropic thermal parameters by full-matrix least-squares procedures on $F^2$. Pertinent crystallographic parameters are summarized in Table 1. CCDC-761908 (**2b**·2MeCN), 761909 (**3b**·2MeCN), and 761910 (**4b**·2MeCN) contain supplementary crystallographic data for this paper. These data can be obtained free of charge from the Cambridge Crystallographic Data Centre via www.ccdc.cam.ac.uk/data_request/cif.

**Potentiometric Measurements.** Potentiometric titrations were carried out at 25 °C using a Metrohm 794 Basic Titrino instrument connected with a Metrohm AG 9101 Herisau pH glass electrode and a ground-joint diaphragm. Before the experiments, standardization was done with aqueous buffer solutions at pH 4.00 and 7.00. Solutions were made up with aqueous methanol (33%, v/v), and the ionic strength was adjusted to 0.1 M by adding appropriate amounts of $NaNO_3$. To compensate for the expected methanol–water liquid junction potential, a correction of 0.051 pH unit was subtracted from the measured pH readings.[26] Computations were carried out with the HYPERQUAD 2000 program, and species distributions were calculated using the program HySS.[27]

To determine the p$K_a$ values of the coordinated water molecules in **2a**–**4a** a typical pH-metric titration was done as follows: 1 mM MeOH/$H_2O$ (33%, v/v) solutions of complexes **2a**–**4a** were titrated with a 0.01 N NaOH solution. The ionic strength of the medium was maintained at $I$ = 0.1 M $NaNO_3$.

**Kinetic Experiments.** Phosphatase-like activities of complexes **2a**–**4a** were determined through the hydrolysis reaction of the model substrate 2-hydroxypropyl-*p*-nitrophenylphosphate (HPNP), under pseudo-first-order conditions (excess complex concentration). In order to determine the activity toward phosphate ester cleavage, the increase of the concentration of *p*-nitrophenolate was followed by UV–vis spectroscopy at 400 nm ($\varepsilon$ = 18 500 M$^{-1}$ cm$^{-1}$), using an Agilent 8453 diode-array spectrophotometer, equipped with an 89090A temperature controller. Observed raw data were fitted according to pseudo-first-order conditions (eq 1), and pseudo-first-order rate


dx.doi.org/10.1021/ic201971t | Inorg. Chem. 2012, 51, 5539–5553

**Table 1. Data Collection and Structure Refinement Parameters for 2b·2MeCN, 3b·2MeCN, and 4b·2MeCN**

| | 2b·2MeCN | 3b·2MeCN | 4b·2MeCN |
|---|---|---|---|
| chem formula | $C_{61}H_{59}BMn_2N_{10}O_5$ | $C_{61}H_{59}BCo_2N_{10}O_5$ | $C_{61}H_{59}BN_{10}O_5Zn_2$ |
| fw | 1132.87 | 1140.85 | 1153.8 |
| cryst size/mm | 0.2 × 0.1 × 0.1 | 0.2 × 0.1 × 0.1 | 0.2 × 0.2 × 0.1 |
| temp/K | 100(2) | 100(2) | 100(2) |
| $\lambda$/Å | 0.710 69 | 0.710 73 | 0.710 69 |
| cryst syst | triclinic | triclinic | triclinic |
| space group (No.) | $P\bar{1}$ (2) | $P\bar{1}$ (2) | $P\bar{1}$ (2) |
| $a$/Å | 11.753(5) | 11.724(5) | 11.704(5) |
| $b$/Å | 15.507(5) | 15.372(5) | 15.424(5) |
| $c$/Å | 16.617(5) | 16.541(5) | 16.578(5) |
| $\alpha$/deg | 85.299(5) | 85.966(5) | 86.301(5) |
| $\beta$/deg | 71.906(5) | 72.133(5) | 72.295(5) |
| $\gamma$/deg | 77.990 (5) | 78.077(5) | 77.886(5) |
| $V$/Å$^3$ | 2815(17) | 2776(17) | 2787.5(17) |
| $Z$ | 2 | 2 | 2 |
| $d_{calcd}$/g cm$^{-3}$ | 1.336 | 1.365 | 1.373 |
| $\mu$/mm$^{-1}$ | 0.507 | 0.657 | 0.920 |
| $F$(000) | 1174 | 1188 | 1198 |
| no. of rflns collcd | 18 897 | 18 722 | 18 806 |
| no. of unique rflns ($R_{int}$) | 13 403 (0.0272) | 13 231 (0.0573) | 13 280 (0.0304) |
| no. of rflns used ($I > 2\sigma(I)$) | 9645 | 7145 | 9439 |
| GOF on $F^2$ | 1.091 | 1.046 | 1.179 |
| final R1, wR2 indices ($I > 2\sigma(I)$)[a,b] | 0.0687, 0.1480 | 0.0879, 0.1546 | 0.0733, 0.1837 |
| R1, wR2 indices (all data)[a,b] | 0.1070, 0.2077 | 0.1684, 0.2154 | 0.1113, 0.2589 |

[a] $R1 = \sum(|F_o| - |F_c|)/\sum|F_o|$. [b] $wR2 = \{\sum[w(|F_o|^2 - |F_c|^2)^2]/\sum[w(|F_o|^2)^2]\}^{1/2}$.

constants ($k_{obs}$) were obtained from the plot of $\ln(a_0/a_0 - x)$ versus $t$, where $a_0$ is the initial concentration of HPNP and $x$ is the amount of $p$-nitrophenolate (PNPate) and $p$-nitrophenol (PNPh) at time $t$.

$$\text{HPNP} \xrightarrow{\text{complex (excess)}} \{\text{PNPate} + \text{PNPh}\}$$

$t = 0$ $a_0$ 0

$t = t$ $a_0 - x$ $x$

Following pseudo-first-order kinetics

$$\ln(a_0/a_0 - x) = k_{obs}t \quad (1)$$

The amount of $p$-nitrophenolate is calculated from the Lambert–Beer law (eq 2)

$$A = \varepsilon cl \quad (2)$$

With regard to the pH-dependent equilibrium between $p$-nitrophenol (PNPh) and $p$-nitrophenolate (PNPate), the increase of the concentration of the reaction product can be calculated (pH = p$K_s$ + log[PNPate]/[PNPh]) by using a p$K_s$ value of 7.15.[9c] The kinetic studies were performed in MeOH/$H_2O$ (33%, v/v). The solution was buffered using HEPES or CHES buffers (20 mM), and the ionic strength was maintained at $I$ = 0.1 M $NaNO_3$. Experiments to determine the dependence of the reaction rate on the complex concentration were carried out at 30 °C, pH 8.50, [HPNP] = 5 × 10$^{-5}$ M, [complex] = 50 × 10$^{-5}$ to 150 × 10$^{-5}$ M, for all three complexes. The effect of temperature on the reaction rate was investigated in the range 30–45 °C at pH 8.50, and a 10-fold excess of complex (50 × 10$^{-5}$ M) relative to substrate (5 × 10$^{-5}$ M) was maintained. The influence of acetate on the reaction rate was evaluated at pH 8.50, 30 °C, and a 10-fold substrate excess (4.62 × 10$^{-4}$ M) relative to the complex (4.62 × 10$^{-5}$ M). In all cases the complex solution was mixed with buffer solution in a thermostated UV cell and was left for 0.5 h for temperature equilibration prior to the addition of substrate. All kinetic experiments were run twice, and average values were taken. In all of these experiments, the spontaneous hydrolysis was corrected by direct difference between two identical parallel reactions, but without addition of catalyst in one of them.

Kinetic data analysis for phosphatase-like activities of complexes **2a**–**4a** were also done following Michaelis–Menten treatment, as before.[20] The data were plotted and treated with the initial rate method. Initial rates were determined from the slope of the tangent to the $p$-nitrophenolate concentration versus time curve at $t$ = 0. The total amount of $p$-nitrophenol/$p$-nitrophenolate was determined by using a p$K_a$ value of 7.15.[9c] The kinetic studies were performed under conditions as described above.

**Monitoring of Hydrolysis Products of HPNP by $^{31}$P NMR.** The hydrolysis of a 2.30 × 10$^{-3}$ M solution of HPNP with 4.62 × 10$^{-5}$ M of the catalyst **4a** was investigated by $^{31}$P NMR at 30 °C in MeOH/$H_2O$ (33%, v/v) buffered with CHES (20 mM) at pH 8.50 and $I$ = 0.1 M $NaNO_3$. The reaction was followed by monitoring the appearance of the signal at 17.98 ppm corresponding to the cyclic phosphodiester formed after the release of $p$-nitrophenolate anion (the chemical shift value is with respect to 85% $H_3PO_4$ as the external standard).

## RESULTS AND DISCUSSION

**Synthesis of the Complexes.** Reactions of $M^{II}(O_2CMe)_2 \cdot xH_2O$ (where M = Mn, Co, and Zn and $x$ = 4 (Mn and Co) or 2 (Zn)) with $HL^2$ in MeOH, followed by addition of $KPF_6$, afforded the isolation of crystalline solids of composition $[M^{II}_2(L^2)(\mu\text{-}O_2CMe)_2(MeCN)_2][PF_6]$ (M = Mn (**2a**), Co (**3a**), Zn (**4a**)). Recrystallization was achieved from MeCN/$Et_2O$. Reactions of $M^{II}(O_2CMe)_2 \cdot xH_2O$ (where M = Mn, Co, Zn and $x$ = 4 (Mn, Co), 2 (Zn)) with $HL^2$ in MeOH followed by addition of $NaBPh_4$ afforded the isolation of crystalline solids of composition $[M^{II}_2(L^2)(\mu\text{-}O_2CMe)_2(MeCN)_2][BPh_4]$ (M = Mn (**2b**), Co (**3b**), Zn (**4b**)). In spite of our sincere attempts single crystals of **2a**–**4a** ($PF_6^-$ salt) could not be obtained. It is for this reason that we synthesized **2b**–**4b** ($BPh_4^-$ salt). The absorption spectral properties of **2a** and **3a** are identical with those of **2b** and **3b**


dx.doi.org/10.1021/ic201971t | Inorg. Chem. 2012, 51, 5539–5553

**Table 2. Selected Bond Lengths (Å) and Angles (deg) in 2b·2MeCN, 3b·2MeCN, and 4b·2MeCN**

| | | | |
|---|---|---|---|
| **2b**·2MeCN | | | |
| Mn1−O1 | 2.103(3) | Mn2−O3 | 2.115(3) |
| Mn1−O2 | 2.166(3) | Mn2−O5 | 2.131(3) |
| Mn1−O4 | 2.103(3) | Mn2−N5 | 2.243(4) |
| Mn1−N1 | 2.283(4) | Mn2−N6 | 2.267(3) |
| Mn1−N2 | 2.221(3) | Mn2−N7 | 2.320(4) |
| Mn1−N8 | 2.364(4) | Mn1···Mn2 | 3.3689(14) |
| Mn2−O1 | 2.102(3) | | |
| O1−Mn1−O2 | 98.02(11) | O1−Mn2−O5 | 103.13(12) |
| O1−Mn1−O4 | 103.57(12) | O1−Mn2−N5 | 88.76(12) |
| O1−Mn1−N1 | 159.36 (12) | O1−Mn2−N6 | 159.33(11) |
| O1−Mn1−N2 | 89.71(12) | O1−Mn2−N7 | 87.81(12) |
| O1−Mn1−N8 | 86.08(12) | O3−Mn2−O5 | 92.44(13) |
| O2−Mn1−O4 | 92.91(13) | O3−Mn2−N5 | 168.04(13) |
| O2−Mn1−N1 | 92.00 (12) | O3−Mn2−N6 | 95.98(12) |
| O2−Mn1−N2 | 90.28(12) | O3−Mn2−N7 | 90.64(12) |
| O2−Mn1−N8 | 175.78(12) | O5−Mn2−N5 | 88.05(13) |
| O4−Mn1−N1 | 93.84(13) | O5−Mn2−N6 | 93.40(13) |
| O4−Mn1−N2 | 165.75(13) | O5−Mn2−N7 | 176.24(13) |
| O4−Mn1−N8 | 87.06(13) | N5−Mn2−N6 | 72.07(13) |
| N1−Mn1−N2 | 72.16(13) | Mn1−O1−Mn2 | 106.46(12) |
| O1−Mn2−O3 | 93.58(12) | | |
| **3b**·2MeCN | | | |
| Co1−O1 | 2.030(4) | Co2−O3 | 2.040(4) |
| Co1−O2 | 2.120(4) | Co2−O5 | 2.107(4) |
| Co1−O4 | 2.015(4) | Co2−N5 | 2.126(5) |
| Co1−N1 | 2.178(5) | Co2−N6 | 2.156(5) |
| Co1−N2 | 2.097(5) | Co2−N7 | 2.184(6) |
| Co1−N8 | 2.206(6) | Co1···Co2 | 3.378(5) |
| Co2−O1 | 2.024(4) | | |
| O1−Co1−O2 | 96.67(16) | O1−Co2−O5 | 93.85(16) |
| O1−Co1−O4 | 98.65(17) | O1−Co2−N5 | 92.06(17) |
| O1−Co1−N1 | 166.30(18) | O1−Co2−N6 | 166.78(17) |
| O1−Co1−N2 | 92.28(18) | O1−Co2−N7 | 90.11(18) |
| O1−Co1−N8 | 89.25(17) | O3−Co2−O5 | 91.89(17) |
| O2−Co1−O4 | 91.15(17) | O3−Co2−N5 | 169.07(18) |
| O2−Co1−N1 | 88.85(17) | O3−Co2−N6 | 93.86(18) |
| O2−Co1−N2 | 89.95(18) | O3−Co2−N7 | 90.40(19) |
| O2−Co1−N8 | 173.94(18) | O5−Co2−N5 | 87.32(18) |
| O4−Co1−N1 | 93.75(18) | O5−Co2−N6 | 89.22(17) |
| O4−Co1−N2 | 168.81(18) | O5−Co2−N7 | 175.06(18) |
| O4−Co1−N8 | 86.70(19) | N5−Co2−N6 | 75.23(18) |
| N1−Co1−N2 | 75.13(19) | Co1−O1−Co2 | 112.83(18) |
| O1−Co2−O3 | 98.87(16) | | |
| **4b**·2MeCN | | | |
| Zn1−O1 | 2.037(3) | Zn2−O3 | 2.033(4) |
| Zn1−O2 | 2.097(3) | Zn2−O5 | 2.074(4) |
| Zn1−O4 | 2.008(3) | Zn2−N5 | 2.153(4) |
| Zn1−N1 | 2.176(4) | Zn2−N6 | 2.156(4) |
| Zn1−N2 | 2.119(4) | Zn2−N7 | 2.304(5) |
| Zn1−N8 | 2.397(5) | Zn1···Zn2 | 3.3689(14) |
| Zn2−O1 | 2.017(3) | | |
| O1−Zn1−O2 | 99.31(13) | O1−Zn2−O5 | 95.41(13) |
| O1−Zn1−O4 | 99.54(14) | O1−Zn2−N5 | 90.62(14) |
| O1−Zn1−N1 | 162.96(14) | O1−Zn2−N6 | 163.74(14) |
| O1−Zn1−N2 | 91.60(14) | O1−Zn2−N7 | 87.82(17) |
| O1−Zn1−N8 | 86.08(12) | O3−Zn2−O5 | 93.53(15) |
| O2−Zn1−O4 | 92.91(13) | O3−Zn2−N5 | 168.40(15) |
| O2−Zn1−N1 | 91.84(14) | O3−Zn2−N6 | 93.35(15) |
| O2−Zn1−N2 | 91.35(15) | O3−Zn2−N7 | 88.92(16) |
| O2−Zn1−N8 | 174.61(14) | O5−Zn2−N5 | 88.43(15) |
| O4−Zn1−N1 | 92.33(15) | O5−Zn2−N6 | 92.06(15) |
| O4−Zn1−N2 | 166.40(14) | O5−Zn2−N7 | 175.52(15) |
| O4−Zn1−N8 | 84.36(15) | N5−Zn2−N6 | 75.14(15) |
| N1−Zn1−N2 | 75.20(15) | Zn1−O1−Zn2 | 106.46(12) |
| O1−Zn2−O3 | 100.57(14) | | |

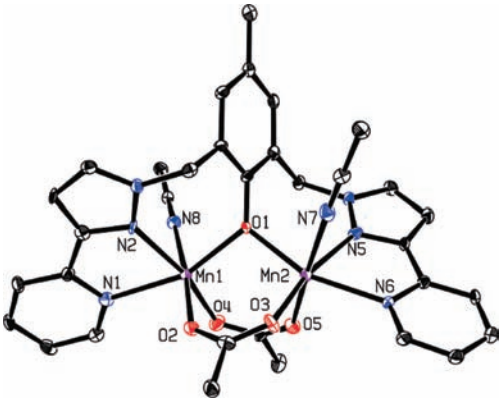


**Figure 1.** Perspective view of the cation $[Mn^{II}_2(L^2)(\mu\text{-}O_2CMe)_2(MeCN)_2]^+$ in the crystal of **2b**·2MeCN. Only donor atoms are labeled. All of the hydrogen atoms are omitted for clarity.

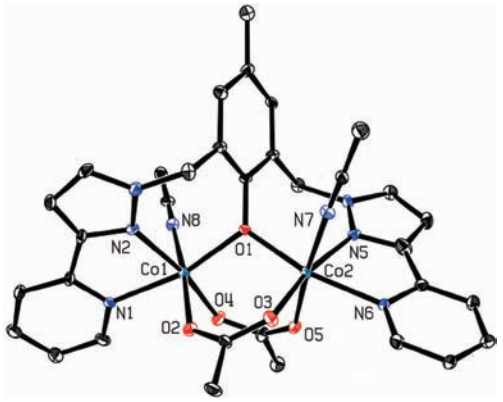


**Figure 2.** Perspective view of the cation $[Co^{II}_2(L^2)(\mu\text{-}O_2CMe)_2(MeCN)_2]^+$ in the crystal of **3b**·2MeCN. Only donor atoms are labeled. All of the hydrogen atoms are omitted for clarity.

(Experimental Section), which suggests that the core structure remains invariant in the two sets of complexes with $PF_6^-$/$BPh_4^-$ anions. Reactivity studies were done with $PF_6^-$ salts, due to solubility reasons. Single crystals grown for structural studies have the compositions $[Mn^{II}_2(L^2)(\mu\text{-}O_2CMe)_2(MeCN)_2][BPh_4]\cdot 2MeCN$ (**2b**·2MeCN), $[Co^{II}_2(L^2)(\mu\text{-}O_2CMe)_2(MeCN)_2][BPh_4]\cdot 2MeCN$ (**3b**·2$CH_3CN$), and $[Zn_2^{II}(L^2)(\mu\text{-}O_2CMe)_2(MeCN)_2][BPh_4]\cdot 2MeCN$ (**4b**·2MeCN).

**General Characterization.** IR spectra displayed characteristic absorptions due to the stretching vibration of coordinated acetate ion: 1607 and 1476 $cm^{-1}$ (**2a**); 1599 and 1475 $cm^{-1}$ (**2b**); 1610 and 1434 $cm^{-1}$ (**3a**); 1605 and 1435 $cm^{-1}$ (**3b**); 1609 and 1439 $cm^{-1}$ (**4a**); 1607 and 1448 $cm^{-1}$ (**4b**).[28] Absorptions are also observed due to uncoordinated $PF_6^-$ and $BPh_4^-$ in **2a**,**b**, **3a**,**b**, and **4a**,**b**, respectively. Elemental analyses, IR, and solution electrical conductivity data (1:1 electrolyte in MeCN)[23]


dx.doi.org/10.1021/ic201971t | Inorg. Chem. 2012, 51, 5539−5553

are in good agreement with the above formulations of the complexes. $^1$H NMR spectra of the diamagnetic complexes **4a,b** (Supporting Information, Figures S1 and S2) neatly establish their solution-state structure. For **4a** the chemical shift values are higher compared to those of **4b**, suggestive of a hydrogen-bonding interaction between the fluorine atom of $PF_6^-$ and ligand H atoms.

**Structural Analysis.** To confirm the structures of the complexes and mode of coordination of the ligand $(L^2)^-$, single-crystal X-ray structure determinations of the complexes was carried out. The complexes are isostructural. Selected bond lengths and bond angles are given in Table 2.

Perspective views of the cationic parts of $[Mn^{II}_2(L^2)(\mu\text{-}O_2CMe)_2(MeCN)_2][BPh_4]\cdot 2MeCN$ (**2b**·2MeCN), $[Co^{II}_2(L^2)(\mu\text{-}O_2CMe)_2(MeCN)_2][BPh_4]\cdot 2MeCN$ (**3b**·2MeCN), and $[Zn^{II}_2(L^2)(\mu\text{-}O_2CMe)_2(MeCN)_2][BPh_4]\cdot 2MeCN$ (**4b**·2MeCN) are displayed in Figures 1 and 2 and Figure S3 (Supporting Information), respectively. Two $M^{II}$ ions are held together by a bridging phenolate oxygen from $(L^2)^-$ and two acetate groups in a $\mu_{1,3}$ bridging mode. Two nitrogen donor atoms from each arm of the ligand and a solvent (MeCN) molecule coordinate facially and complete the distorted-octahedral $N_3O_3$ coordination about each $M^{II}$ ion. Notably, N(pyridyl)−M−N(pyrazole) bite angles are quite acute (72.07(13)−72.16(13)° for **2b**·2MeCN, 75.13(19)−75.23(18)° for **3b**·2MeCN and 75.14(15)−75.20(15)° for **4b**·2MeCN), due to the presence of a directly attached five-membered ring and a six-membered heterocyclic ring in the 3-(2-pyridyl)pyrazole unit. The bridging acetates are staggered relative to each other. Moreover, each acetate ion is coordinated to two $M^{II}$ ions asymmetrically (Table 2). A similar observation applies for $M^{II}$−N bond distances, with $M^{II}$−$NCCH_3$ distances being the longest and $M^{II}$−N(pyrazole) distances being the shortest.

A discussion on comparable metric parameters is in order. The $M^{II}$−O (2.102(3)−2.166(3) Å for $Mn^{II}$, 2.015(4)−2.120(4) Å for $Co^{II}$, 2.008(3)−2.097(3) Å for $Zn^{II}$) and M−N(pyridyl and pyrazole) (2.221(3)−2.283(4) Å for $Mn^{II}$, 2.097(5)−2.178(5) Å for $Co^{II}$, 2.119(4)−2.176(4) Å for $Zn^{II}$) distances follow the trend expected, on the basis of changes in the numbers of d electrons. Moreover, the distances fall within the range commonly observed in analogous $Mn^{II}$,[29−34] $Co^{II}$,[35] and $Zn^{II}$ complexes.[36,37] The $M^{II}$−O(phenolate)−$M^{II}$ angles follow the trend: 106.46(12)° for **2b**·2MeCN, 112.83(18)° for **3b**·2MeCN, and 106.46(12)° for **4b**·2MeCN. The M···M separations are comparable: 3.3689(4) Å for **2b**·2MeCN, 3.378(5) Å for **3b**·2MeCN, and 3.3689(14) Å for **4b**·2MeCN.

**Absorption Spectra.** Yellow MeCN solutions of **2b** display two strong bands at 290 nm ($\varepsilon \approx 34\,000$ $M^{-1}$ $cm^{-1}$) and at 245 nm ($\varepsilon \approx 50\,000$ $M^{-1}$ $cm^{-1}$), assigned to metal-perturbed intraligand transitions (Supporting Information, Figure S4). The absorption spectral feature of **3b** in MeCN (Supporting Information, Figure S5) clearly supports the presence of six-coordinate $Co^{II}$ centers in solution.[38,39] Three spin-allowed d−d transitions are expected for octahedral $Co^{II}$, unless the field strength of the ligands are such that $^4A_{2g}$ and $^4T_{1g}(P)$ terms have the same energy.[38] For **3a** the assignment of $\nu_2$ at 510 nm ($\varepsilon = 140$ $M^{-1}$ $cm^{-1}$) to the $^4T_{1g}(F) \rightarrow {}^4A_{2g}(F)$ transition is unequivocal and the $\nu_3$ band at 470 nm ($\varepsilon = 135$ $M^{-1}$ $cm^{-1}$) is assigned to the $^4T_{1g}(F) \rightarrow {}^4T_{1g}(P)$ transition.[38b] Still higher energy transitions at 287 nm ($\varepsilon \approx 15\,000$ $M^{-1}$ $cm^{-1}$) and 241 nm (sh) ($\varepsilon \approx 36\,000$ $M^{-1}$ $cm^{-1}$) are due to metal-perturbed intraligand transitions.

**ESI-MS Spectra.** Although X-ray structural studies have been done on the $BPh_4^-$ salts **2b**·MeCN, **3b**·MeCN, and **4b**·MeCN, due to enhanced solubility in MeOH/$H_2O$ medium (33%, v/v) $PF_6^-$ salts of the cations of **2a**−**4a** have been used for potentiometric titration and phosphate ester hydrolysis studies. To provide proof of our contention that **2a,b**, **3a,b**, and **4a,b** have common core structures (cf. Absorption Spectra) and they differ only in the nature of the counteranion, we investigated the ESI-MS spectral behavior of **2a,b** (Supporting Information, Figure S6), **3a,b** (Supporting Information, Figure S7), and **4a,b** (Supporting Information, Figure S8), along with identification of major/minor species present in solution and their simulated spectra. The data analysis reveals the following. The major species present in solution are $[Mn^{II}_2(L^2)(\mu\text{-}O_2CMe)(OMe)]^+$ (**2a,b**), $[Co^{II}_2(L^2)(\mu\text{-}O_2CMe)_2]^+$ and $[Co^{II}_2(L^2)(\mu\text{-}O_2CMe)(HCO_2)]^+$ (**3a**), $[Co^{II}_2(L^2)(\mu\text{-}O_2CMe)(OMe)]^+$ (**3b**), and $[Zn^{II}_2(L^2)(\mu\text{-}O_2CMe)(OMe)]^+$ and $[Zn^{II}_2(L^2)(\mu\text{-}O_2CMe)(HCO_2)]^+$ (**4a,b**). The minor species present in solution have been identified as $[Co^{II}_2(L^2)(\mu\text{-}O_2CMe)(OMe)]^+$ (**3a**) and $[Zn^{II}_2(L^2)(\mu\text{-}O_2CMe)(HCO_2)]^+$ (**3b**).

**Magnetic Studies.** The magnetic measurements of $[Mn^{II}_2(L^2)(\mu\text{-}O_2CMe)_2(MeCN)_2][BPh_4]$ (**2b**) were carried out in the temperature range 2−300 K. A plot of $\chi_M$ and $\chi_M T$ versus $T$ (per two $Mn^{II}$ ions) is illustrated in Figure 3. The value of $\chi_M T$ at 300 K is 7.73 $cm^3$ $mol^{-1}$ K ($\mu_{eff}$/Mn = 5.31 $\mu_B$). It decreases upon cooling and practically vanishes at low temperature. The $\chi_M$ curve presents a maximum at 32 K. The room-temperature magnetic moment is lower than the spin-only value of a high-spin $d^5$ ion ($\mu_{eff}$/Mn = 5.92 $\mu_B$). This behavior is typical of an antiferromagnetically coupled system. The experimental data are fitted by employing the expression derived from the isotropic Heisenberg−Dirac−van Vleck (HDvV) spin-exchange Hamiltonian $H = -JS_1\cdot S_2$ ($S_1 = S_2 = {}^5/_2$) (eq 3), where $x = J/kT$. The best least-squares fitting of experimental data is obtained with $g = 2.00(1)$ and $J = -8.50(2)$ $cm^{-1}$. The negative value of $J$ indicates an antiferromagnetic coupling between the two $Mn^{II}$ centers.

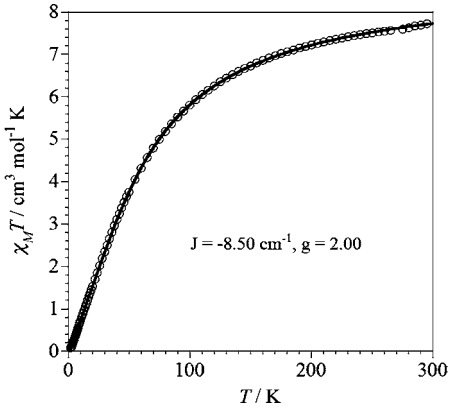


**Figure 3.** Plot of $\chi_M T$ versus $T$ for a powdered sample of **2b**. The solid line represents the best theoretical fit, described in the text.

Dinuclear $Mn^{II}$ complexes with a $\mu$-oxo(phenolate) and bis-$\mu_{1,3}$-carboxylate (*syn-syn* conformation) bridges (see Scheme 1) typically show magnetic exchange coupling constants in the range −4.4 to −9.8 $cm^{-1}$, as shown in Table 3. In this table we have given magneto-structural results of reported examples containing $\mu$-oxo (phenolate/acetate/water) and bis-$\mu_{1,3}$-carboxylate (acetate/benzoate) (*syn-syn* conformation) bridges between


dx.doi.org/10.1021/ic201971t | *Inorg. Chem.* 2012, 51, 5539−5553

**Scheme 1**

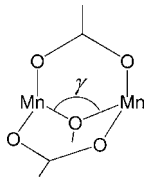


**Table 3. Magneto-Structural Parameters for $Mn^{II}$ Complexes Containing a $\mu$-Oxo (Phenolate/Acetate/Water) and Bis-$\mu_{1,3}$-carboxylate (Benzoate/Acetate) (*syn-syn* Conformation) Bridges between the Two $Mn^{II}$ Ions (see Scheme 1)**

| $-J/cm^{-1}$ | $d$(Mn···Mn)/Å | $\gamma$(Mn−O−Mn)/deg | $\mu$-oxo | $\mu$-carboxylato | ref |
|---|---|---|---|---|---|
| 9.8 | 3.41 | 107.9 | phenolate | acetate | 33c |
| 9.0 | 3.39 | 107.0 | phenolate | benzoate | 30 |
| 8.8 | 3.45 | 110.6 | phenolate | acetate | 33a |
| 8.6 | 3.42 | 108.7 | phenolate | benzoate | 33a |
| 8.6 | 3.47 | 109.5 | phenolate | acetate | 31a, b, 33c |
| 8.5 | 3.37 | 106.5 | phenolate | acetate | this work |
| 8.0 | 3.33 | 101.2 | phenolate | acetate | 29a |
| 7.2 | 3.45 | 106.4 | phenolate | acetate | 33b |
| 6.8 | 3.37 | 101.9 | phenolate | acetate | 40 |
| 6.4 | 3.38 | 102.3 | phenolate | acetate | 29b |
| 5.8 | 3.60 | 113.5 | phenolate | benzoate | 29c |
| 5.7 | 3.86 | 113.3 | water | benzoate | 41 |
| 5.5 | 3.56 | 112.5 | phenolate | acetate | 31b |
| 5.0 | 3.34 | 100.3 | phenolate | acetate | 40 |
| 4.4 | 3.61 | 112.2 | acetate | acetate | 42 |

two $Mn^{II}$ ions (see Scheme 1). Some authors[31] suggested a relationship between the magnetic exchange coupling constant ($J$) and intramolecular metal−metal separation $d$(Mn···Mn) (Table 3) and concluded that $|J|$ decreases as $d$(Mn···Mn) increases. With the examples in Table 3 a working relationship is roughly observed. It is well-known that the $\mu_{1,3}$-carboxylate bridge in the *syn-syn* conformation always mediates antiferromagnetic coupling.[43,44] In the case of the $\mu$-oxo bridge, ferro- or antiferromagnetic coupling is observed, depending on the value of the angle at the bridgehead ($\gamma$).[43,45] The larger the value of $\gamma$, the greater the antiferromagnetic coupling. In the given examples the $\gamma$ values are larger than 100°. Hence, an antiferromagnetic coupling is predicted through this bridge. There is another correlation between the values of $d$(Mn···Mn) and $\gamma$ (the greater the value of $d$, the larger is $\gamma$). Consequently, one would expect that greater $d$(Mn···Mn) values (and then larger $\gamma$) would result in stronger antiferromagnetic interactions, in contrast to what is roughly observed (Table 3). A possible explanation for this disagreement would be the well-documented counter-complementary effect[46] between these two types of bridges.[47] This effect shows that as the antiferromagnetic coupling through the $\mu$-oxo bridge increases (larger $\gamma$ values), it counterbalances the antiferromagnetic interaction through the $\mu_{1,3}$-carboxylate (*syn-syn* conformation), the result being a decrease in the overall antiferromagnetic interaction. Along this line, even a ferromagnetic interaction could be expected for the larger $\gamma$ values.[47b,c] This point may be illustrated by the corresponding dicobalt(II) complex (compound **3**, see below), where the $\gamma$ value is 112.8°, which leads to an overall ferromagnetic coupling ($J$ = +2.51 $cm^{-1}$). In summary, in order to understand the trend of $J$ values in these complexes, apart from the small structural variations at the two types of bridges, one has to consider also the counter-complementary effect.

$$\chi_M = \frac{2N\beta^2 g^2}{kT}\left\{\frac{e^x + 5e^{3x} + 14e^{6x} + 30e^{10x} + 55e^{15x}}{1 + 3e^x + 5e^{3x} + 7e^{6x} + 9e^{10x} + 11e^{15x}}\right\} \quad (3)$$

The value of $\mu_{eff}$/Mn for **2b** in MeCN solution (300 K) was determined by using the NMR method to examine whether or not the solid-state structure is retained in solution. The solution-state value (5.07 $\mu_B$) is somewhat smaller than the solid-state value (5.31 $\mu_B$). This behavior could be due to a relaxed geometry in the solution state, allowing a better pathway for the magnetic coupling.

The magnetic measurements of $[Co^{II}_2(L^2)(\mu\text{-}O_2CMe)_2(MeCN)_2][BPh_4]$ (**3b**) were carried out in the temperature range 2−300 K. The $\chi_M T$ versus $T$ plot is shown in Figure 4. At room temperature, $\chi_M T$ (per two Co atoms) is 5.93 $cm^3$ $mol^{-1}$ K

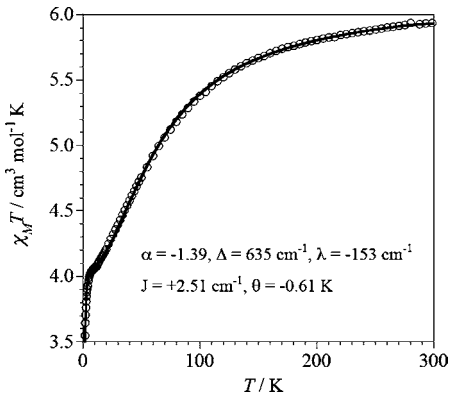


**Figure 4.** Plot of $\chi_M T$ versus $T$ for a powdered sample of **3b**. The solid line represents the best theoretical fit, described in the text.

**Scheme 2**

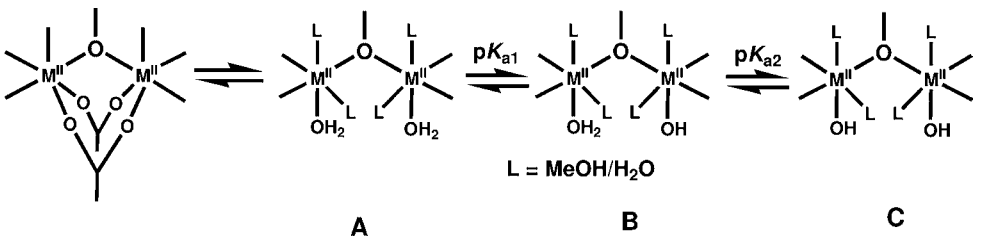



dx.doi.org/10.1021/ic201971t | Inorg. Chem. 2012, 51, 5539−5553

($\mu_{eff}$/Co = 4.87 $\mu_B$), a value which decreases to 3.54 cm$^3$ mol$^{-1}$ K at 2 K ($\mu_{eff}$/Co = 3.76 $\mu_B$). The $\mu_{eff}$/Co value (= 4.87 $\mu_B$) at room temperature is larger than the spin-only value of a high-spin $d^7$ ion (3.87 $\mu_B$; $\mu_{SO} = [4S(S + 1)]^{1/2}$; $S = {}^3/_2$). This indicates a contribution of the orbital angular momentum typical for the $^4T_{1g}$ ground term.[48] The magnetic moment decreases upon cooling, as expected for the depopulation of the higher energy spin−orbit levels. An incipient plateau is observed at ca. 10 K with a value of $\chi_M T$ at about 4.06 cm$^3$ mol$^{-1}$ K ($\mu_{eff}$/Co = 4.03 $\mu_B$) and then decreases until 3.54 cm$^3$ mol$^{-1}$ K at 2 K ($\mu_{eff}$/Co = 3.76 $\mu_B$). At low temperature ($T$ < 20 K), only the ground Kramers doublet is populated and it can be regarded as an effective spin doublet $S_{eff} = {}^1/_2$ with a $g$ value in the range 3.9−4.3, the value for this ground Kramers doublet being in the range 3.4−3.7 $\mu_B$.[49] Note that these values are smaller than that corresponding to the incipient plateau at ca. 10 K (ca. 4.03 $\mu_B$) and close to the smallest value observed at 2 K (3.76 $\mu_B$). These features suggest the occurrence of a weak intramolecular ferromagnetic interaction (which would produce a minimum in the $\chi_M T$ curve and a further increase at low temperatures) as well as a weak intermolecular antiferromagnetic interaction (which would account for the lack of the increase of $\chi_M T$ at lower temperatures).[50] The full Hamiltonian describing the magnetic properties of **3b** is given by eq 4.[49b] The first term takes into account the magnetic exchange interaction between the two spin quartets ($S = {}^3/_2$) from each $Co^{II}$ ion. The second one describes the spin−orbit coupling, where $\alpha$ is an orbital reduction factor defined as $\alpha = Ak$ (the $k$ parameter considers the reduction of the orbital momentum caused by the delocalization of the unpaired electron, and $A$ contains the admixture of the upper $^4T_{1g}(^4P)$ state into the $^4T_{1g}(^4F)$ ground state). The third term takes into account an axial distortion of the octahedral geometry around the $Co^{II}$ ions. Such axial distortion splits the triplet orbital ground state $^4T_{1g}$ into a singlet $^4A_2$ and a doublet $^4E$ level with an energy gap of $\Delta$, which is positive when the orbital singlet is the lowest and negative for the reverse case. The last term is the Zeeman interaction. In order to simplify the calculation, we took advantage of the isomorphism between the orbital triplet $T_1$ (coming from the $^4F$ term) and the triplet $L = 1$ from a $P$ term. This means that $\|\mathbf{T_1}\| = -\alpha\|\mathbf{P}\|$.[48b] No analytical expression for the magnetic susceptibility as a function of $J$, $\lambda$, $\alpha$, and $\Delta$ can be derived.[49,51] The matrix-diagonalization technique[52] allowed us to determine the values of these parameters. A corrective term ($\Theta$) in the form $T - \Theta$ was also introduced to take into account intermolecular interactions. The best-fit parameters are $J$ = +2.51(2) cm$^{-1}$, $\alpha$ = 1.39(2), $\lambda$ = −153(3) cm$^{-1}$, $\Delta$ = 635(5) cm$^{-1}$, and $\Theta$ = −0.61(2) K.

$$\hat{H} = -J\hat{S}_1\hat{S}_2 - \sum_{i=1}^{2} \alpha\lambda\hat{L}_i\hat{S}_i + \sum_{i=1}^{2} \Delta[\hat{L}_{zi}^2 - 2/3] + \beta H \sum_{i=1}^{2} (-\alpha\hat{L}_i + g_e\hat{S}_i) \quad (4)$$

The value of $A$ can be determined from the crystal-field parameters $Dq$ (cubic ligand-field parameter) and $B$ (interelectronic repulsion) through eqs 5 and 6, where $c$ is the mixing coefficient.[49b]

In the weak crystal-field limit ($B \gg Dq$), $c = 0$ and $A = 1.5$ (values used in most of the magnetic studies of $Co^{II}$), whereas in the strong crystal-field limit ($B \ll Dq$), $c = -{}^1/_2$ and $A = 1$. The values of $Dq \approx 1060$ cm$^{-1}$ and $B \approx 930$ cm$^{-1}$ were determined from the peaks observed in the electronic spectra of **3a,b** ($\nu_2$ = 19 600 cm$^{-1}$ and $\nu_3$ = 21 300 cm$^{-1}$; cf. Absorption Spectra).[38b] From these values and using eqs 5 and 6, values of $c = -0.20$ and $A = 1.40$ can be obtained. A value of 0.99 for $k$ is deduced from the values of $\alpha$ = 1.39 and $A$ = 1.4. It is worth mentioning here that the value of $Dq$ is 1020 cm$^{-1}$ for the corresponding phenoxo-/acetato-bridged $Ni^{II}$ dimeric complex,[20] justifying the $Dq$ and $B$ values obtained here. The fact that the value of $\lambda$ (= −153 cm$^{-1}$) is slightly smaller than that of the free ion value ($\lambda_0$ = −180 cm$^{-1}$); this is due to a covalency effect.[40] The values of the parameters obtained by this fit are within the range of those reported for high-spin octahedral $Co^{II}$ complexes.[49−51] The calculated curve matches very well with the experimental data in the whole temperature range (Figure 4) and it unambiguously shows the existence of an intramolecular ferromagnetic interaction between the $Co^{II}$ ions. The different nature of the magnetic coupling found in **3b** in comparison to that observed in **2b** (see Table 3) must be attributed to the larger value of $\gamma$ (which would effectively counterbalance the antiferromagnetic coupling through the bis-$\mu_{1,3}$-carboxylate bridges) as well as to the different numbers of magnetic orbitals involved. In this sense, $J$ = −0.4 cm$^{-1}$ has been observed for an analogous dicobalt(II) complex (with a $\mu$-oxo(phenolate) and bis-$\mu_{1,3}$-acetate (*syn-syn* conformation) bridge between the two $Co^{II}$ ions).[35] In this case, the $\gamma$ angle is 112.2°, a value somewhat smaller than that observed in **2b**·2MeCN ($\gamma$ = 112.8°); therefore, this complex still exhibits an antiferromagnetic coupling that is very weak in magnitude ($J$ = −0.4 cm$^{-1}$). Finally, two dicobalt(II) complexes, one of them having a bis-$\mu$-oxo (phenolate) bridge ($\gamma$ = 102°)[35b,53] and the other one with a $\mu$-oxo (phenolate) ($\gamma$ = 120°) and a $\mu_{1,3}$-acetate (*syn-syn* conformation) bridge,[35b] could be illustrative for the relative importance of each type of bridge on the overall magnetic coupling. The $J$ value for the former is −5.2 cm$^{-1}$, whereas that for the latter is −7.3 cm$^{-1}$. The first example reveals that a $\gamma$ value as small as 102° already mediates a relatively important antiferromagnetic coupling ($J$ = −5.2 cm$^{-1}$). In contrast, the second example with a much larger $\gamma$ value (120°) has a somewhat greater antiferromagnetic coupling ($J$ = −7.3 cm$^{-1}$) due to the counterbalance effect of a single $\mu_{1,3}$-acetate (*syn-syn* conformation).

$$A = \frac{3/2 - c^2}{1 + c^2} \quad (5)$$

$$c = 0.75 + 1.875\frac{B}{Dq} - 1.25\left[1 + 1.8\frac{B}{Dq} + 2.25\left(\frac{B}{Dq}\right)^2\right]^{1/2} \quad (6)$$

The $\mu_{eff}$/Co value for **3b** in MeCN solution (300 K) is 4.67 $\mu_B$, a value which is somewhat below that in the solid state (4.83 $\mu_B$); this behavior is similar to that observed for **2b**.

**Potentiometric Titrations.** The species distribution in solution is crucial for understanding any hydrolytic reactivity. Potentiometric titrations were performed to determine the p$K_a$ values of the coordinated water molecules in **2a**−**4a** in MeOH/$H_2O$ (33%, v/v; the ionic strength was maintained at $I$ = 0.1 M $NaNO_3$) solutions, because of the low solubility of these


dx.doi.org/10.1021/ic201971t | Inorg. Chem. 2012, 51, 5539−5553

compounds in pure water. Typical curves obtained from the titrations of **3a** with 0.01 N NaOH are shown in Figure 5, and

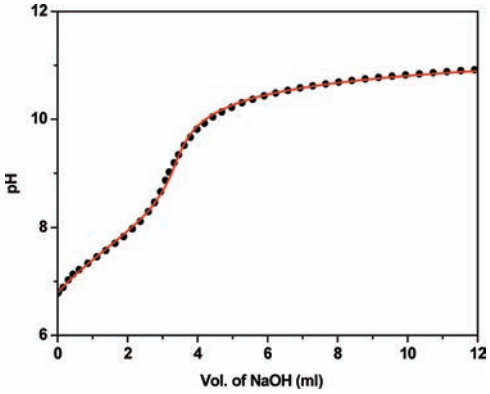


**Figure 5.** Representative titration curve obtained by titrating $[Co^{II}_2(L^2)(\mu\text{-}O_2CMe)_2(MeCN)_2][PF_6]$ (**3a**) in 33% (v/v) MeOH/$H_2O$ with 0.01 N NaOH. The experimental points (black dots) are in good agreement with the theoretical curve (red line).

those of **2a** and **4a** are shown in Figures S9 and S10, respectively (Supporting Information). It is understandable that the coordinated solvent molecules present in the solid of **2a**–**4a** would not remain coordinated and are expected to be replaced by water molecule(s), under the experimental conditions. The results obtained for the complexes show the neutralization of 2 mol of NaOH/mol of the complex in the pH range 6–11. On treatment of the data, two deprotonation constants were thus obtained for each complex. The distribution curve for **3a** is displayed in Figure 6, and those of **2a** and **4a** are shown in Figures S11 and S12, respectively (Supporting Information). The p$K_a$ values of the coordinated water molecules were calculated to be 7.67 ± 0.08 and 8.69 ± 0.06 for **2a**, 7.09 ± 0.05 and 8.05 ± 0.06 for **3a**, and 6.20 ± 0.04 and 6.80 ± 0.03 for **4a**.

We[20] and others[7] have demonstrated that for bis-$\mu_2$-1,3-acetato dinickel(II) systems supported by endogenous phenolate bridges the acetate ions do not remain coordinated to the nickel(II) centers at pH 9.00 and are replaced by water molecules. Given this observation for other closely similar bimetallic systems,[7] we believe that for the complexes **2a**–**4a** at pH 8.50 a similar situation would prevail under the experimental conditions employed in the kinetic experiments of this investigation (see below). In fact, $^1$H NMR spectral data of **4a** in $CD_3OD/D_2O$ (60/40, v/v) show a signal at 1.96 ppm, due to free acetate ion (Supporting Information, Figure S13). This experiment justifies our contention.

From the potentiometric titration data (see above), we are inclined to believe that the two p$K_a$ values observed for **2a**–**4a** are due to the conversion of "$M^{II}(H_2O)M^{II}(H_2O)$" to "$M^{II}(H_2O)$-$M^{II}(OH)$" species (p$K_{a1}$) and of "$M^{II}(H_2O)M^{II}(OH)$" to "$M^{II}$-$(OH)M^{II}(OH)$" species (p$K_{a2}$) (Scheme 2).[20]

**Phosphate Ester Hydrolysis.** In recent years a number of investigations have been made to investigate the potential of dimetal(II) complexes with vacant labile coordination site(s) for the hydrolysis of phosphate esters.[1d,3–18,20] The requirements for the catalytically active site of a synthetic hydrolase have also been identified.[7,20] The complexes **2a**–**4a** (cf. Structural Analysis for **2b**–**4b**) have two labile sites for substrate binding and to provide an $H_2O/OH^-$ as the nucleophile and hence are ideal candidates for exploring their potential to catalyze the hydrolysis of an organophosphate

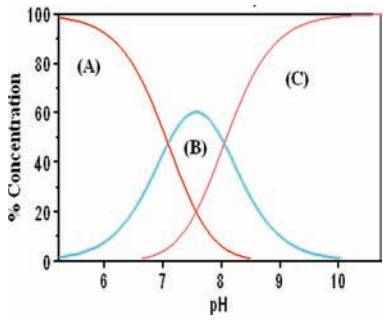


**Figure 6.** Species distribution curves of $[Co^{II}_2(L^2)(\mu\text{-}O_2CMe)_2(MeCN)_2][PF_6]$ (**3a**) in 33% (v/v) MeOH/$H_2O$ as a function of pH.

ester. To test the activity of complexes **2a**–**4a** toward phosphate ester hydrolysis, 2-hydroxypropyl-*p*-nitrophenyl-phosphate (HPNP) was used following the protocol reported earlier.[20] HPNP releases *p*-nitrophenolate by intramolecular nucleophilic attack of the appended hydroxide group and formation of a cyclic phosphodiester (Scheme 3). The formation

**Scheme 3**

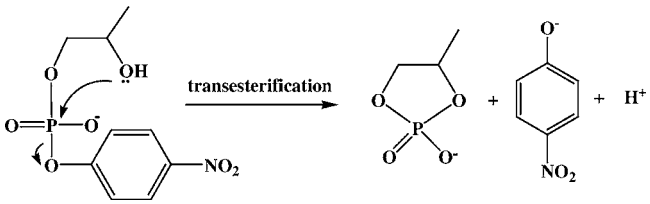


of a cyclic phosphodiester product has been authenticated by $^{31}$P NMR spectroscopy. The hydrolysis of HPNP by complex **4a** was monitored by a time-dependent $^{31}$P NMR spectral study. $^{31}$P NMR spectra obtained under conditions of excess substrate (see above) at various time intervals are given in Figure S14 (Supporting Information). The chemical shift of HPNP is at −5.17 ppm. As the hydrolysis reaction proceeds, the formation of the cyclic phosphodiester is observed at 17.98 ppm. At longer times ($t$ = 36 h) almost all the substrates are hydrolyzed to a cyclic phosphodiester.

To investigate the phosphatase-like activity, experiments have been carried out by monitoring spectrophotometrically the absorption increase of the liberated *p*-nitrophenolate anion ($\lambda_{max}$ = 400 nm with $\varepsilon$ = 18 500 $M^{-1}$ $cm^{-1}$; considering equilibration *p*-nitrophenol/*p*-nitrophenolate (p$K_a$ = 7.15)),[9c] under pseudo-first-order conditions (excess complex; this condition was followed for **1a**).[5a,20] The hydrolysis reaction of HPNP by complexes **2a**–**4a** has been investigated, under pseudo-first-order conditions (excess complex concentration at 30 °C).[5a,20] The time course of the change in the absorbance for the hydrolysis of HPNP by **2a** at different concentrations is displayed in Figure S15 (Supporting Information).[54] In the first set of experiments the pH dependence of catalytic activities was investigated in the pH range 7.0–9.5 for all the complexes (Figure 7). It is interesting to note that the rate constant ($k_{obs}$) versus pH plots for **2a**–**4a** do not have well-behaved sigmoidal shapes, which is characteristic of a kinetic process controlled by acid–base equilibria, as observed before for **1a**.[20] Although the curves are still sigmoidal, the rate enhancement starts at much higher pH. Thus, the observed behavior does not appear to be associated with the formation of the species **C**, particularly in the case of **4a** (p$K_a$ values: 6.20 ± 0.04 and 6.80 ± 0.03)


dx.doi.org/10.1021/ic201971t | Inorg. Chem. 2012, 51, 5539–5553

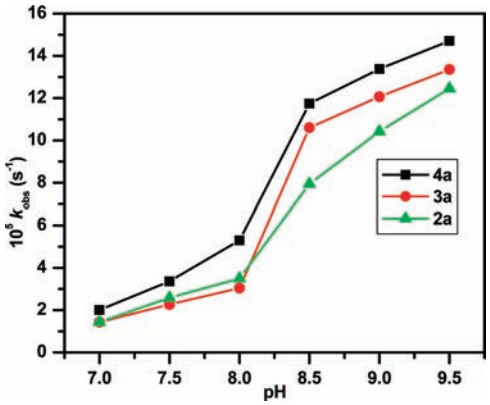


**Figure 7.** Dependence of the rate constant ($k_{obs}$) on pH for hydrolysis of HPNP promoted by complexes **2a**–**4a**. Conditions: [complex] = $50 \times 10^{-5}$ M, [HPNP] = $5 \times 10^{-5}$ M, [buffer] = $20 \times 10^{-3}$ M (CHES, pH 8.50); $I$ = 0.1 M ($NaNO_3$) in MeOH/$H_2O$ (33%, v/v).

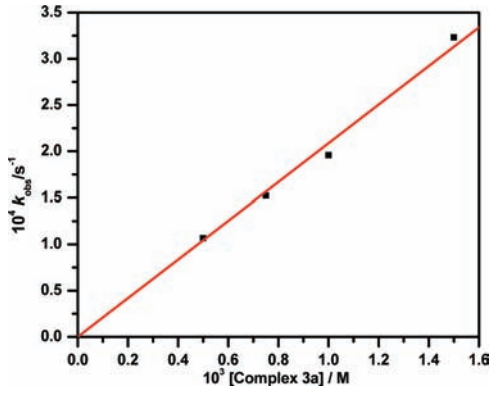


**Figure 8.** Dependence of the reaction rate on the concentration of the complex $[Co^{II}_2(L^2)(\mu\text{-}O_2CMe)_2(MeCN)_2][PF_6]$ (**3a**) for the hydrolysis of HPNP. Conditions: [HPNP] = $5 \times 10^{-5}$ M; [complex] = (50–125) $\times 10^{-5}$ M; buffer CHES (pH 8.50), $I$ = 0.1 M ($NaNO_3$) in MeOH/$H_2O$ (33%, v/v) at 30 °C.

(Scheme 2). The enhanced rate that is observed above pH 8 could be a result of pre-equilibrium deprotonation of the hydroxyl moiety of the substrate HPNP.[9d] Metal coordination of this hydroxyl moiety is necessary in order to induce a sufficiently low p$K_a$ value to achieve complete protolysis at pH 8.0–9.5. For a noncoordinated 2′-hydroxyl group of an analogue of HPNP that contains a ribose unit and an ethyl group on the phosphate, a p$K_a$ value of 12.8 has been determined.[55] The difference in p$K_a$ for noncoordinated HPNP is expected to be small. In fact, a lowering of 3–4 units upon coordination could be feasible, given the fact that water coordinated to hydrated Zn(II) reduces its p$K_a$ to 9.6.[56]

To identify the species present in solution, under the conditions of our measurement (MeOH/$H_2O$ (33%, v/v) at pH 8.5), for complexes **2a**–**4a** ESI-MS+ spectral analyses were carried out with excess substrate concentration (complex/HPNP = 1/30). The results for **2a**–**4a** are displayed in Figures S17–S19, respectively (Supporting Information). Analysis of ESI-MS+ spectra points toward the generation of solvated species along with metal-coordinated HPNP species, on the basis of the simulated mass and isotopic distribution pattern. For **2a** the peak at $m/z$ 842.05 corresponds to the species $[Mn^{II}_2(L^2)(HPNP)(H_2O)_2]^+$ (Scheme 4; Supporting Information, Figure S17). Other peaks at $m/z$ 753.15 and 779.98 are attributed to the species $\{[Mn^{II}_2(L^2)(O_2CMe)(H_2O)][PF_6]\}^+$ and $[\{[Mn^{II}_2(L^2)(MeOH)(H_2O)_4][PF_6]\}^{2+} + e^-]^+$, respectively. For **3a** the peaks at $m/z$ 964.86 and 872.87 correspond to the species $\{[Co^{II}_2(L^2)(HPNP)(OMe)(MeOH)_3] + Na^+\}^+$ and $\{[Co^{II}_2(L^2)(HPNP)(H_2O)_2]^+ + Na^+ + e^-\}^+$, respectively (Scheme 4). The peak at $m/z$ 712.95 corresponds to the solvated species $\{[Co^{II}_2(L^2)(O_2CMe)(MeOH)_3(H_2O)]^{2+} + e^-\}^+$. ESI-MS+ spectra for **4a** show a peak at $m/z$ 886.07 corresponding to the species $\{[Zn^{II}_2(L^2)(O_2CMe)(HPNP)] + H^+\}^+$ and another peak at $m/z$ 747.05 attributed to the species $[\{[Zn^{II}_2(L^2)(OH)(MeOH)][PF_6]\}^+ + 2e^- + 2H^+\}^+$. Thus, ESI-MS+ spectral data point to the fact that acetate ions are prone to be liberated under the experimental conditions and also support the fact that during complex–substrate interaction, coordination by the deprotonated hydroxyl group of HPNP to the metal center takes place (Schemes 2 and 4).

**Scheme 4**

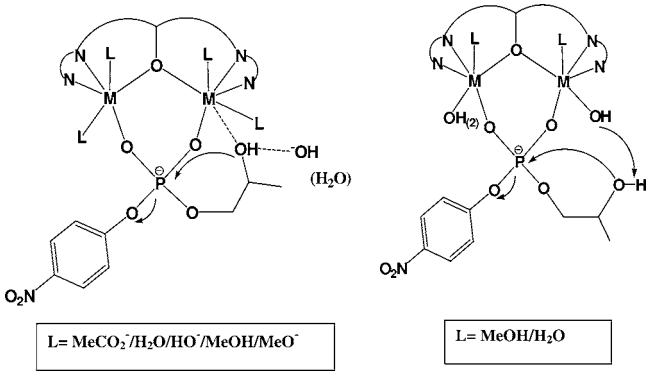


The kinetic data reveal that for **2a**–**4a** the rate of hydrolysis is linearly dependent on the concentration of the complex: **2a** (Supporting Information, Figure S20), **3a** (Figure 8), and **4a** (Supporting Information, Figure S21). The apparent second-order rate constants ($k_2$, $M^{-1}$ $s^{-1}$) were calculated from the slope of the straight lines of $k_{obs}$ versus [complex]: 0.152 ± 0.086 (**2a**), 0.208 ± 0.042 (**3a**), and 0.230 ± 0.063 (**4a**). It is important to note that complex **4a** is more reactive than complex **3a**, followed by **2a** (Table 4). It is worth mentioning that the corresponding value for **1a** is 0.058 ± 0.002 $M^{-1}$ $s^{-1}$.[20] No significant hydrolysis of the test substrate occurred when the metal complex was absent.

**Table 4. Observed Pseudo-First-Order Rate Constants for Hydrolysis/Transesterification of HPNP in MeOH/$H_2O$ (33%, v/v) Buffer CHES at pH 8.50, $I$ = 0.1 M ($NaNO_3$), 30 °C with [catalyst] = $50 \times 10^{-5}$ M and [HPNP] = $5 \times 10^{-5}$ M**

| cat. | $k_{obs}$ ($10^{-5}$ $s^{-1}$) | $k_{obs}/k_{uncat.}$ |
|---|---|---|
| **1a**[a] | 2.96 ± 0.32 | 130.97 ± 2.84 |
| **2a** | 7.96 ± 0.84 | 352.21 ± 12.06 |
| **3a** | 10.66 ± 0.92 | 471.68 ± 19.02 |
| **4a** | 12.10 ± 1.02 | 535.39 ± 21.72 |
| uncat. | 0.0226 | 1 |

[a]Reference 20.

To investigate further the effect of substrate (HPNP) concentration on hydrolysis reactions catalyzed by complexes **2a**–**4a**, kinetic data analyses were also done by the Michaelis–Menten method (excess substrate concentration at pH 8.5 and 30 °C, under saturation kinetics conditions). The plots of the initial reaction rate versus the concentration of HPNP


dx.doi.org/10.1021/ic201971t | Inorg. Chem. 2012, 51, 5539–5553

and Lineweaver–Burk plots (double-reciprocal plots) are displayed in Figures S22–S25, respectively (Supporting Information) for **2a** and **3a**. The corresponding plots for **4a** are displayed in Figures 9 and Figure 10. The initial reaction rate versus concentration of HPNP plot attains saturation as the concentration of HPNP increases, suggesting formation of a complex–substrate intermediate in the course of the reaction. The kinetic parameters are summarized in Table 5. Analysis of the data reveals that the Michaelis–Menten constant for **4a** ($K_M$ = 2.14 ± 0.43 mM) is higher compared to those for **1a**–**3a**, indicating less binding affinity ($K_{ass}$ = 467.28 ± 78 $M^{-1}$) and hence a higher catalytic rate constant ($k_{cat}$ = 3.44 ± 0.45 × $10^{-4}$ $s^{-1}$) in comparison to those for **1a**–**3a**. Since the $Zn^{II}$ ion is the most Lewis acidic, it will activate HPNP better than other metal ions and hence exhibit a higher catalytic activity. However, the binding affinity of HPNP for **4a** is stronger than those for other similar types of dinuclear Zn complexes having alkoxide or phenolate bridging groups ($K_M$ = 5.4–16 mM).[9d] Consequently, the $k_{cat}$ values for the HPNP transesterification reaction catalyzed by **4a** is comparable to that reported in the literature (6.4 × $10^{-4}$ to 0.01 $s^{-1}$)[9d] and it is (15.22 ± 0.26) × $10^2$ times ($k_{cat}/k_{uncat}$) that of the uncatalyzed reaction.

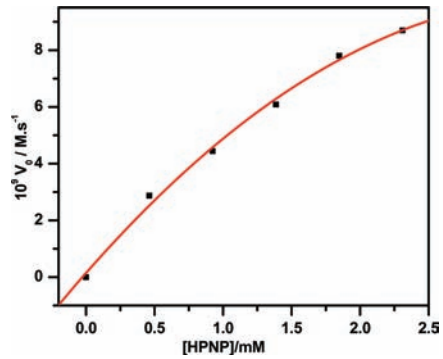


**Figure 9.** Dependence of the initial reaction rate ($V_0$) on the HPNP concentration for the hydrolysis reaction promoted by $[Zn^{II}_2(L^2)(\mu\text{-}O_2CMe)_2(MeCN)_2][PF_6]$ (**4a**). Conditions: [complex] = 4.62 × $10^{-5}$ M; [buffer] = 20 × $10^{-3}$ M (CHES, pH = 8.50); $I$ = 0.1 M ($NaNO_3$) in MeOH/$H_2O$ (33%, v/v) at 30 °C.

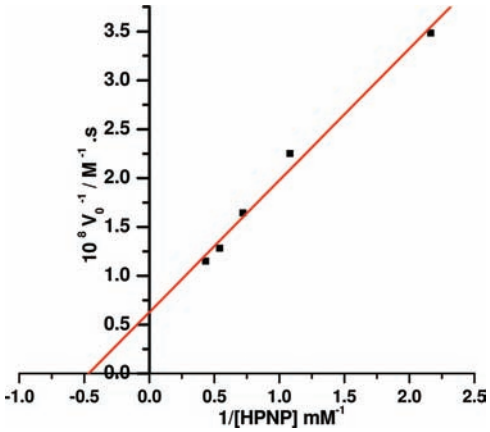


**Figure 10.** Lineweaver–Burk plot for the hydrolysis reaction promoted by $[Zn^{II}_2(L^2)(\mu\text{-}O_2CMe)_2(MeCN)_2][PF_6]$ (**4a**). Conditions: [complex] = 4.62 × $10^{-5}$ M; [buffer] = 20 × $10^{-3}$ M (CHES, pH = 8.50); $I$ = 0.1 M ($NaNO_3$) in MeOH/$H_2O$ (33%, v/v) at 30 °C.

Interestingly, the values of the second-order rate constant for **2a**–**4a** (Table 4) are comparable to the catalytic efficiency values $k_{cat}/K_M$ (0.170 $M^{-1}$ $s^{-1}$ for **2a**, 0.194 $M^{-1}$ $s^{-1}$ for **3a**, and 0.161 $M^{-1}$ $s^{-1}$ for **4a**), obtained from the kinetic studies under Michaelis–Menten conditions (Table 5). The corresponding value for **1a** was determined to be 0.089 $M^{-1}$ $s^{-1}$.[20] Thus, the rate of hydrolysis of HPNP under identical experimental conditions by phenoxo-bridged dimeric $Mn^{II}$ (**2a**), $Co^{II}$ (**3a**), $Ni^{II}$ (**1a**), and $Zn^{II}$ (**4a**) complexes, terminally supported by a 3-(2-pyridyl)pyrazole unit ($(L^2)^-$), follows the order **4a** > **3a** > **2a** > **1a**. Notably, this trend follows the decrease of p$K_a$ values of $M^{II}$-coordinated water (7.95 ± 0.04 and 8.78 ± 0.03 for **1a**,[20] 7.67 ± 0.08 and 8.69 ± 0.06 for **2a**, 7.09 ± 0.05 and 8.05 ± 0.06 for **3a**, and 6.20 ± 0.04 and 6.80 ± 0.03 for **4a**). This fact indicates that the higher the Lewis acidity of $M^{II}$ ion, the faster the rate of hydrolysis. A similar result has been observed for $Zn^{II}$ complexes in the hydrolysis of 2,4-dinitrophenyl diethyl phosphate and diphenyl 4-nitrophenyl phosphate.[17a,b] Since the Lewis acidity of the $Zn^{II}$ complex is higher, coordination/activation of substrate HPNP is easier. Accordingly, this suggests that HPNP hydrolysis by the present set of closely similar complexes proceeds via a concerted mechanism, in which the substrate HPNP coordinates to the $M^{II}$ ion (in the case of the $Zn^{II}$ complex, deprotonation of a coordinated pendant hydroxyl group of HPNP is augmented by pH greater than 8), followed by an attack of the $M^{II}$-coordinated $OH^-$ ion on the coordinated HPNP (see below).

Understandably, for any complex to act as an efficient catalyst for hydrolysis of the substrate, the incoming substrate should first get bound effectively to the catalyst, which is dictated by a combination of geometrical and electronic factors of the metal–ligand interactions. In the present case, during this process the hydroxyl group of HPNP is activated by the coordination to metal ions and in turn is deprotonated before its nucleophilic attack on the phosphorus center (Scheme 4). The $Zn^{II}$ ion, being the most Lewis acidic in the chosen set of complexes, is expected to activate the hydroxyl group of HPNP better than others. Thus, **4a** is found to be a better promoter of hydrolysis/transesterification of HPNP in comparison to **1a**–**3a**.

To investigate the effect of acetate ion, which is partially or fully released under the conditions of our potentiometric titrations and kinetic experiments (cf. ESI-MS+ results), on the rate of hydrolysis of HPNP by complexes **2a**–**4a**, the hydrolysis reaction was monitored as a function of acetate concentration. Figure S26 (Supporting Information) shows the percentage of inhibition on the hydrolysis reaction versus equivalents of acetate added. It is found that acetate ions inhibit the hydrolysis reaction, as determined earlier.[7,20] When the acetate concentration equals the substrate concentration, a reduction of the rate by 27% for **2a**, 31% for **3a**, and 34% for **4a** is observed. With addition of 20 equiv of acetate ions such values reach 45% for **2a**, 48% for **3a**, and 54% for **4a**. These results support the finding (see above) that the acetate ions are prone to be released during hydrolysis experiments. A similar result was observed in the case of $Ni^{II}$ complex **1a**.[20]

The dependence of temperature (30–45 °C) on the rate of hydrolysis of HPNP by complexes **2a**–**4a** was also investigated under the experimental conditions employed in the kinetics experiments. The activation energies and parameters $E_a$, $\Delta H^{\ddagger}$, $\Delta S^{\ddagger}$, and $\Delta G^{\ddagger}$ (Table 6) were obtained through the Arrhenius and Eyring equations. Figures S27 and S28 (Supporting Information) and Figure 11 show the linearization of the observed rate constants ($k_{obs}$) for the reactions catalyzed by


dx.doi.org/10.1021/ic201971t | Inorg. Chem. 2012, 51, 5539–5553

**Table 5. Results of Michaelis–Menten Treatment**

| complex | $V_{max} \times 10^9$ (M $s^{-1}$) | $K_M \times 10^3$ (M) | $k_{cat} \times 10^4$ ($s^{-1}$) | $K_{assoc}$ ($M^{-1}$) | $E$ ($M^{-1}$ $s^{-1}$) | $f \times 10^{-2}$ |
|---|---|---|---|---|---|---|
| **1a**[a] | 6 ± 1.68 | 1.46 ± 0.28 | 1.30 ± 0.35 | 684.93 ± 110 | 0.089 ± 0.01 | 5.75 ± 0.69 |
| **2a** | 7 ± 1.58 | 0.926 ± 0.20 | 1.58 ± 0.34 | 1079.91 ± 120 | 0.17 ± 0.05 | 6.90 ± 0.60 |
| **3a** | 12.20 ± 1.64 | 1.38 ± 0.33 | 2.64 ± 0.34 | 724.63 ± 139.43 | 0.194 ± 0.02 | 11.60 ± 0.04 |
| **4a** | 15.90 ± 2.17 | 2.14 ± 0.43 | 3.44 ± 0.45 | 467.28 ± 78 | 0.161 ± 0.01 | 15.22 ± 0.26 |

[a]Reference 20.

**Table 6. Activation Parameters for the Hydrolysis of HPNP**

| complex | $E_A$ (kJ $mol^{-1}$) | $A$ ($s^{-1}$) (frequency factor) | $k_{obs}$ ($10^{-5}$ $s^{-1}$) | $\Delta H^{\ddagger}$ (kJ $mol^{-1}$) | $\Delta S^{\ddagger}$ (J $mol^{-1}$ $K^{-1}$) | $\Delta G^{\ddagger a}$ (kJ $mol^{-1}$) |
|---|---|---|---|---|---|---|
| **1a**[b] | 71.00 ± 4.60 | $3.75 \times 10^7$ ± 5.15 | 2.16 | 68.00 ± 4.65 | −109.00 ± 13 | 101.00 ± 8.58 |
| **2a** | 67.95 ± 5.71 | $4.36 \times 10^7$ ± 9.15 | 8.41 | 65.40 ± 5.72 | −107.30 ± 16 | 97.91 ± 10.56 |
| **3a** | 62.60 ± 4.46 | $6.92 \times 10^6$ ± 5.62 | 11.27 | 60.00 ± 4.47 | −122.54 ± 14 | 97.18 ± 8.87 |
| **4a** | 67.80 ± 3.25 | $5.93 \times 10^7$ ± 3.53 | 11.80 | 65.29 ± 3.26 | −104.67 ± 10 | 97.00 ± 6.29 |

[a]$\Delta G^{\ddagger} = \Delta H^{\ddagger} - T\Delta S^{\ddagger}$, at 30 °C. [b]Reference 20.

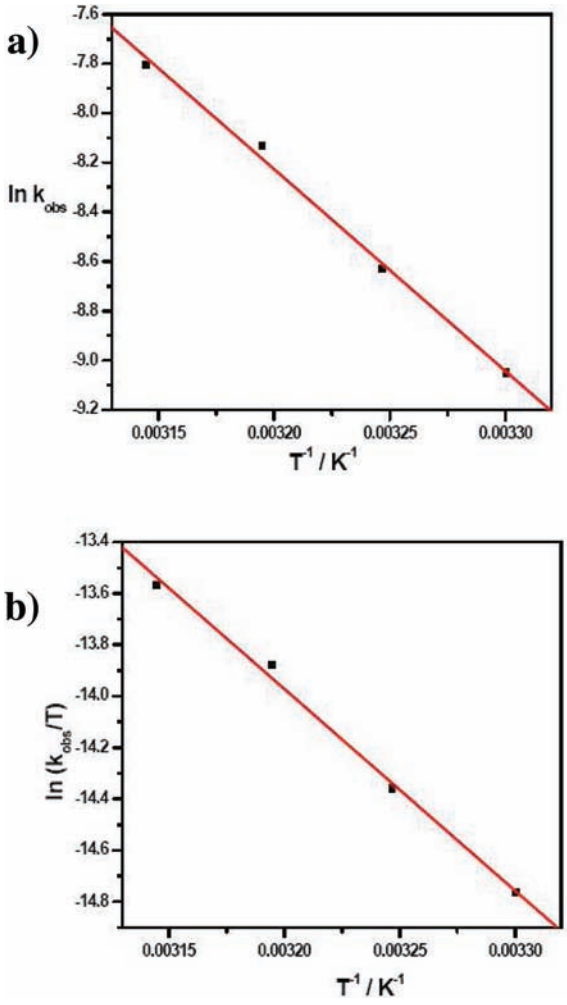


**Figure 11.** Linearizations of the observed rate constants for the hydrolysis of HPNP ($5 \times 10^{-5}$ M) promoted by $[Zn^{II}_2(L^2)(\mu\text{-}O_2CMe)_2(MeCN)_2][PF_6]$ (**4a**) ($50 \times 10^{-5}$ M) as a function of temperature: (a) Arrhenius equation; (b) Eyring equation. Conditions: [buffer] = $20 \times 10^{-3}$ M (CHES, pH = 8.50); $I$ = 0.1 M ($NaNO_3$) in $MeOH/H_2O$ (33%, v/v).

complexes **2a**–**4a**, respectively. The $E_a$ values for all the complexes are comparable, suggesting a closely similar reaction barrier and thereby a similar course of reaction.

Notably, in all cases $\Delta S^{\ddagger} < 0$, which indicates that an organization of the reactive species occurs in the transition state. In other words, the transesterification reaction proceeds through a transition state involving interaction/adduct formation between the catalyst and HPNP. Also in all cases, $\Delta H^{\ddagger} > 0$, reflecting bond breaking in the activated complex. This is associated with nucleophilic attack on the electrophilic phosphorus atom, which causes release of the cyclic phosphate and *p*-nitrophenolate. Therefore, the thermodynamic parameters obtained from temperature-dependent studies reveal that essential steps in this reaction are as follows: first the activation of HPNP by the catalyst through binding to the metal center(s) and then intramolecular nucleophilic attack on the electrophilic phosphorus atom with release of the leaving groups. With the values of $E_a$ and $A$ obtained from the Arrhenius equation, the $k_{obs}$ values ($s^{-1}$) were calculated and the values (Table 6) are found to be 8.41 (**2a**), 11.27 (**3a**), and 11.80 (**4a**). The corresponding value for **1a** is 2.16.[20] These values are quite comparable to the $k_{obs}$ values obtained from kinetic experiments (Table 4: 2.96 (**1a**),[20] 7.96 (**2a**), 10.66 (**3a**), and 12.10 (**4a**)). Thus, the thermodynamic parameters point toward the following order for the hydrolysis of HPNP: **4a** > **3a** > **2a** > **1a**. This is in agreement with the observed reaction rates.

Finally, the following comments on the hydrolysis of phosphate esters by metallohydrolases in general and hydrolysis/transesterification of HPNP by synthetic dimetal(II) complexes in particular are in order. The commonly accepted mechanism of the metal ion catalyzed hydrolysis of phosphate esters involves the following key steps: deprotonation of a metal-bound species to form the effective nucleophile, binding of the substrate to the metal center(s), intramolecular nucleophilic attack on the electrophilic phosphorus atom with the release of the leaving group, and possibly regeneration of the catalyst. It should be mentioned here that although a large number of studies on HPNP transesterification have been reported, a definitive assessment of the mechanism of the reaction assisted by metal ions has still not been made.[14] From the present study we can conclude that the substrate coordination is an essential requisite for the hydroxyl group of HPNP to be activated by the metal ion and, as a consequence, HPNP gets deprotonated for further attack of the electrophilic phosphorus atom, causing hydrolysis/transesterification of HPNP. The organic phosphate ester coordinates to the dimetal(II) complex, possibly bridging through the phosphate group. Direct coordination to the dimetal site activates the P–O bond for nucleophilic attack, and


dx.doi.org/10.1021/ic201971t | Inorg. Chem. 2012, 51, 5539–5553

it is prominent for the dizinc(II) complex because of its high Lewis acidity in comparison to that of other first-row transition-metal ions.

The catalytic activity of a metal ion is largely governed by its Lewis acidity. The stronger the Lewis acidity, the larger the effect of the metal ion on substrate activation. An increase in the Lewis acidity of a metal ion in turn results in a decrease of the nucleophilicity of a metal-bound hydroxide ion. In this work we demonstrate that the stronger the Lewis acidity ($Z_{eff}/r$) of the metal ion, the more acidic the $M^{II}$-coordinated water, and the larger the propensity of the metal ion to catalyze hydrolysis of an activated phosphate ester HPNP. Notably, the observed $k_2$ values for $Mn^{II}$ (**2a**), $Co^{II}$ (**3a**), and $Zn^{II}$ (**4a**) complexes linearly correlate with $Z_{eff}/r$ values[19] of the metal ion (Figure 12). Because $Zn^{II}$ has a

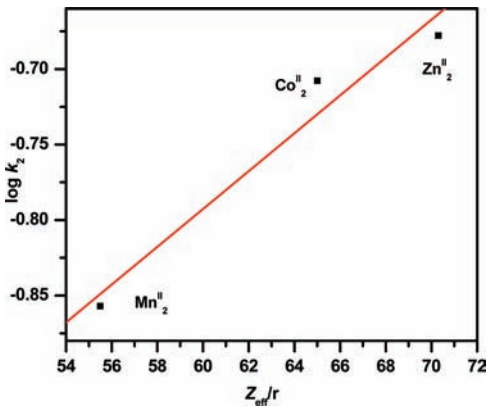


**Figure 12.** Linearizations of log $k_2$ with $Z_{eff}/r$ for the hydrolysis of HPNP.

$d^{10}$ electronic configuration, its polarizing effect is isotropic, leading to flexible coordination. In contrast, the binding of ligands is rather directional and restricted in the case of $Ni^{II}$. This limits the ways in which ligands (substrates) might bind to $Ni^{II}$ for further reaction. This could be the reason why the $Ni^{II}$ complex (**1a**) does not fit in this line. On the other hand, $Co^{II}$ is well-known for its ability to substitute without loss of activity for $Zn^{II}$ in zinc enzymes. This justifies the observed trend.[19]

Kinetic results for phosphate ester (HPNP) hydrolysis, viewed together with the speciation of complexes **1a**[20] and **2a**−**4a** determined by potentiometric titrations, allow us to propose a classical double Lewis acid activation mechanism. The rates of HPNP hydrolysis increase with an increase of pH from 4 to 9 (Figure 7). An increase in pH also causes an increase in the concentration of the nucleophile (free or $M^{II}$-coordinated $OH^-$ ions). This work strengthens the generally accepted mechanism, which involves the coordination of the substrate to the metal ion, and concerted action of the double Lewis acid activation and the intramolecular general base catalysis by a metal-bound/free hydroxide ion along with pre-equilibrium deprotonation of the hydroxyl moiety of the substrate by the coordination to metal ions prior to the nucleophilic attack on the phosphorus center (Scheme 4).

## SUMMARY AND CONCLUDING REMARKS

In this work, we have synthesized and characterized dinuclear $M^{II}$ (where M = Mn, Co, Zn) complexes with the deprotonated form of 2,6-bis[3-(pyridin-2-yl)pyrazol-1-ylmethyl]-4-methylphenol. In these complexes each metal(II) center has an $M^{II}N_3O_3$ distorted-octahedral coordination sphere, provided by two nitrogens (pyrazole and pyridine) and a bridging phenolate oxygen from the ligand, two other oxygens by bridging acetates, and the sixth coordination site by solvent MeCN. This has given us a unique opportunity to investigate the effect of such a coordination sphere on spectroscopic and magnetic properties (antiferromagnetic coupling between $Mn^{II}_2$ ions, $J = -8.5$ $cm^{-1}$; ferromagnetic coupling between $Co^{II}_2$ ions, $J = +2.5$ $cm^{-1}$).

In an attempt to evaluate the effect of metal ions, i.e. which metal ion is likely to be more efficient in hydrolyzing the model substrate 2-hydroxypropyl-*p*-nitrophenylphosphate (HPNP), detailed kinetic experiments were carried out under pseudo-first-order conditions (excess complex concentration) as well as under excess substrate conditions (Michaelis−Menten kinetic analysis). Results found throughout these experiments revealed that $Zn^{II}_2$ complex **4a** is the most efficient in hydrolyzing HPNP, in comparison to $Mn^{II}_2$ (**2a**), $Co^{II}_2$ (**3a**) or $Ni^{II}_2$ (**1a**). This fact indicates that the higher the Lewis acidity of the $M^{II}$ ion (as judged by $pK_a$ values of $M^{II}$-coordinated water), the faster the rate of hydrolysis. While the pH dependence of the activity toward the hydrolysis of HPNP by **1a** suggested that the $Ni^{II}$-bound hydroxide ion serves as the nucleophile for phosphate ester hydrolysis,[20] a similar situation does not occur for **2a**−**4a**. The pH-dependent rate profiles for **2a**−**4a** suggest a pre-equilibrium deprotonation of the hydroxyl moiety of the substrate by the coordination to metal ions prior to the nucleophilic attack on the phosphorus center (Scheme 4).

## ASSOCIATED CONTENT

### Supporting Information

$^1$H NMR spectra of **4a**,**b** (Figures S1 and S2), X-ray structure of the cationic part of **4b**·2MeCN (Figure S3), absorption spectra of **2b** and **3b** (Figures S4 and S5), ESI-MS+ spectra of **2a**,**b**, **3a**,**b**, and **4a**,**b** (Figures S6−S8), potentiometric titration curves of **2a** and **4a** (Figures S9 and S10), species distribution curves of **2a** and **4a** (Figures S11 and S12), $^1$H NMR spectrum of **4b** in $CD_3OD/D_2O$ (60/40, v/v) (Figure S13), $^{31}$P NMR spectra of the product of HPNP hydrolysis by **4a** at different time intervals (Figure S14), time course for the change in the absorbance by **2a** for HPNP hydrolysis (Figure S15), fitting of raw data to a pseudo-first-order mechanism in the case of **2a** for the hydrolysis of HPNP (Figure S16), ESI-MS+ spectral results of **2a**−**4a**, under hydrolysis conditions (Figure S17−S19), dependence of the reaction rate on the concentration of **2a** and **4a** for the hydrolysis of HPNP (Figures S20 and S21), kinetic studies of the hydrolysis of HPNP under Michaelis−Menten conditions, including the dependence of the initial reaction rate on the HPNP concentration for the hydrolysis reaction by **2a** and **3a** (Figures S22 and S24) and Lineweaver−Burk plots for HPNP hydrolysis catalyzed by **2a** and **3a** (Figures S23 and S25), percentage inhibition of the hydrolysis reaction of HPNP substrate with acetate catalyzed by **2a**−**4a** (Figure S26), and linearizations of the observed rate constants for the hydrolysis of HPNP promoted by **2a** and **3a** as a function of temperature with the Arrhenius equation and Eyring equation (Figures S27 and S28). This material is available free of charge via the Internet at http://pubs.acs.org.

## AUTHOR INFORMATION

### Corresponding Author

*Tel: +91-512-2597437. Fax: +91-512-2597436. E-mail: rnm@iitk.ac.in.


dx.doi.org/10.1021/ic201971t | *Inorg. Chem.* 2012, 51, 5539−5553

### Notes

The authors declare no competing financial interest.

### Present Address

[§]Indian Institute of Science Education and Research Kolkata, Mohanpur Campus, Mohanpur 741 252, India.

## ■ ACKNOWLEDGMENTS

This work was supported by the Department of Science & Technology (DST), Government of India ,and by the Ministerio de Educación y Ciencia (MEC, Spain; projects CTQ2007-61690 and Consolider-Ingenio in Molecular Science CSD2007-00010). R.M. sincerely thanks the DST for a J. C. Bose fellowship. H.A. gratefully acknowledges the award of an SRF, and S.K.B. acknowledges the award of a JRF by the Council of Scientific & Industrial Research, Government of India. We thank Dr. R. Gurunath for his help in fitting the pseudo-first-order data. The comments of the reviewers were very helpful at the revision stage.

## ■ REFERENCES

(1) (a) Sträter, N.; Lipscomb, W. N.; Klabunde, T.; Krebs, B. *Angew. Chem., Int. Ed. Engl.* **1996**, *35*, 2024−2055. (b) Dismukes, G. C. *Chem. Rev.* **1996**, *96*, 2909−2926. (c) Wilcox, D. E. *Chem. Rev.* **1996**, *96*, 2435−2458. (d) Belle, C.; Pierre, J.-L. *Eur. J. Inorg. Chem.* **2003**, 4137−4146. (e) Averill, B. A. In *Comprehensive Coordination Chemistry II: From Biology to Nanotechnology*; McCleverty, J. A., Meyer, T. J., Eds.; Elsevier/Pergamon: Amsterdam, 2004; Vol. *8* (Que, L., Jr., Tolman, W. B., Eds.), pp 641−676. (f) Weston, J. *Chem. Rev.* **2005**, *105*, 2151−2174.

(2) (a) Halcrow, M. A.; Christou, G. *Chem. Rev.* **1994**, *94*, 2421−2481. (b) Lipscomb, W. N.; Sträter, N. *Chem. Rev.* **1996**, *96*, 2375−2433. (c) Perkin, G. *Chem. Rev.* **2004**, *104*, 699−767.

(3) Mitić, N.; Smith, S. J.; Neves, A.; Guddat, L. W.; Gahan, L. R.; Schenk, G. *Chem. Rev.* **2006**, *106*, 3338−3363.

(4) (a) Chin, J. *Acc. Chem. Res.* **1991**, *24*, 145−152. (b) Suh, J. *Acc. Chem. Res.* **1992**, *25*, 273−279. (c) Chin, J. *Curr. Opin. Chem. Biol.* **1997**, *1*, 514−521. (d) Hegg, E. L.; Burstyn, J. N. *Coord. Chem. Rev.* **1998**, *173*, 133−165. (e) Komiyama, M.; Sumaoka, J. *Curr. Opin. Chem. Biol.* **1998**, *2*, 751−757. (f) Krämer, R. *Coord. Chem. Rev.* **1999**, *182*, 243−261. (g) Williams, N. H.; Takasaki, B.; Wall, M.; Chin, J. *Acc. Chem. Res.* **1999**, *32*, 485−493. (h) Kimura, E. *Curr. Opin. Chem. Biol.* **2000**, *4*, 207−213. (i) Morrow, J. R.; Iranzo, O. *Curr. Opin. Chem. Biol.* **2004**, *8*, 192−200. (j) Mancin, F.; Scrimin, P.; Tecilla, P.; Tonellato, U. *Chem. Commun.* **2005**, 2540−2548. (k) Meyer, F. *Eur. J. Inorg. Chem.* **2006**, 3789−3800. (l) Jarenmark, M.; Carlsson, H.; Nordlander, E. *C. R. Chim.* **2007**, *10*, 433−462. (m) Mancin, F.; Tecilla, P. *New J. Chem.* **2007**, *31*, 800−817. (n) Liu, C.; Wang, L. *Dalton Trans.* **2009**, 227−239. (o) Gahan, L. R.; Smith, S. J.; Neves, A.; Schenk, G. *Eur. J. Inorg. Chem.* **2009**, 2745−2758.

(5) (a) Volkmer, D.; Hommerich, B.; Griesar, K.; Haase, W.; Krebs, B. *Inorg. Chem.* **1996**, *35*, 3792−3803. (b) Yamaguchi, K.; Akagi, F.; Fujinami, S.; Suzuki, M.; Shionoya, M.; Suzuki, S. *Chem. Commun.* **2001**, 375−376.

(6) (a) Bonfá, L.; Gatos, M.; Mancin, F.; Tecilla, P.; Tonelatto, U. *Inorg. Chem.* **2003**, *42*, 3943−3949. (b) Livieri, M.; Mancin, F.; Saielli, G.; Chin, J.; Tonellato, U. *Chem. Eur. J.* **2007**, *13*, 2246−2256.

(7) Greatti, A.; Scarpellini, M.; Peralta, R. A.; Casellato, A.; Bortoluzzi, A. J.; Xavier, F. R.; Jovito, R.; de Brito, M. A.; Szpoganicz, B.; Tomkowicz, Z.; Rams, M.; Haase, W.; Neves, A. *Inorg. Chem.* **2008**, *47*, 1107−1119 and references therein.

(8) (a) Albedyhl, S.; Averbuch-Pouchot, M. T.; Belle, C.; Krebs, B.; Pierre, J.-L.; Saint-Aman, E.; Torelli, S. *Eur. J. Inorg. Chem.* **2001**, 1457−1464. (b) Albedyhl, S.; Schnieders, D.; Jancsó, A.; Gajda, T.; Krebs, B. *Eur. J. Inorg. Chem.* **2002**, 1400−1409.

(9) (a) Carlsson, H.; Haukka, M.; Nordlander, E. *Inorg. Chem.* **2004**, *43*, 5681−5687. (b) Carlsson, H.; Haukka, M.; Bousseksou, A.; Latour, J.-M.; Nordlander, E. *Inorg. Chem.* **2004**, *43*, 8252−8262. (c) Jarenmark, M.; Kappen, S.; Haukka, M.; Nordlander, E. *Dalton Trans.* **2008**, 993−996. (d) Jarenmark, M.; Csapó, E.; Singh, J.; Wöckel, S.; Farkas, E.; Meyer, F.; Haukka, M.; Nordlander, E. *Dalton Trans.* **2010**, 8183−8194. (e) Jarenmark, M.; Haukka, M.; Demeshko, S.; Tuczek, F.; Zuppiroli, L.; Meyer, F.; Nordlander, E. *Inorg. Chem.* **2011**, *50*, 3866−3887.

(10) (a) Bauer-Siebenlist, B.; Meyer, F.; Farkas, E.; Vidovic, D.; Dechert, S. *Chem. Eur. J.* **2005**, *11*, 4349−4360. (b) Penkova, L. V.; Maciag, A.; Rybak-Akimova, E. V.; Haukka, M.; Pavlenko, V. A.; Iskenderov, T. S.; Kozłowski, H.; Meyer, F.; Fritsky, I. O. *Inorg. Chem.* **2009**, *48*, 6960−6971.

(11) Selmeczi, K.; Michel, C.; Milet, A.; Gautier-Luneau, I.; Philouze, C.; Pierre, J- L.; Schnieders, D.; Rompel, A.; Belle, C. *Chem. Eur. J.* **2007**, *13*, 9093−9106.

(12) Belousoff, M. J.; Graham, B.; Spiccia, L. *Eur. J. Inorg. Chem.* **2008**, 4133−4139.

(13) (a) Chapman, W. H. Jr.; Breslow, R. *J. Am. Chem. Soc.* **1995**, *117*, 5462−5469. (b) Mohamed, M. F.; Neverov, A. A.; Brown, R. S. *Inorg. Chem.* **2009**, *48*, 11425−11433.

(14) Coleman, F.; Hynes, M. J.; Erxleben, A. *Inorg. Chem.* **2010**, *49*, 6725−6733.

(15) (a) Herschlag, D.; Jencks, W. P. *J. Am. Chem. Soc.* **1987**, *109*, 4665−4674. (b) De Rosch, M. A.; Trogler, W. C. *Inorg. Chem.* **1990**, *29*, 2409−2416. (c) Morrow, J. R.; Buttrey, L. A.; Berback, K. A. *Inorg. Chem.* **1992**, *31*, 16−20. (d) Iranzo, O.; Kovalevsky, A. Y.; Morrow, J. R.; Richard, J. P. *J. Am. Chem. Soc.* **2003**, *125*, 1988−1993. (e) Iranzo, O.; Richard, J. P.; Morrow, J. R. *Inorg. Chem.* **2004**, *43*, 1743−1750.

(16) (a) He, C.; Lippard, S. J. *J. Am. Chem. Soc.* **2000**, *122*, 184−185. (b) Kaminskaia, N. V.; He, C.; Lippard, S. J. *Inorg. Chem.* **2000**, *39*, 3365−3373.

(17) (a) Fujii, Y.; Itoh, T.; Onodera, K.; Tada, T. *Chem. Lett.* **1995**, 305−306. (b) Itoh, T.; Fujii, Y.; Tada, T.; Yoshikawa, Y.; Hisada, H. *Bull. Chem. Soc. Jpn.* **1996**, *69*, 1265−1274. (c) Itoh, T.; Hisada, H.; Usui, Y.; Fujii, Y. *Inorg. Chim. Acta* **1998**, *283*, 51−60.

(18) Koike., T.; Kimura, E. *J. Am. Chem. Soc.* **1991**, *113*, 8935−8941.

(19) Ochiai, E.-I. *J. Chem. Educ.* **1988**, *65*, 943−946.

(20) Mandal, S.; Balamurugan, V.; Lloret, F.; Mukherjee, R. *Inorg. Chem.* **2009**, *48*, 7544−7556.

(21) Amoroso, A. J.; Thompson, A. M. C.; Jeffery, J. C.; Jones, P. L.; McCleverty, J. A.; Ward, M. D. *J. Chem. Soc., Chem. Commun.* **1994**, 2751−2752.

(22) Brown, D. M.; Usher, D. A. *J. Chem. Soc.* **1965**, 6558−6564.

(23) Geary, W. J. *Coord. Chem. Rev.* **1971**, *7*, 81−122.

(24) Evans, D. F. *J. Chem. Soc.* **1959**, 2003−2005.

(25) Farrugia, L. J. *WinGX version 1.64, An Integrated Systems of Windows Programs for the Solution, Refinement and Analysis of Single-Crystal X-ray Diffraction Data*; Department of Chemistry, University of Glasgow, Glasgow, Scotland, 2003.

(26) Bates, R. G.; Paabo, M.; Robinson, R. A. *J. Phys. Chem.* **1963**, *67*, 1833−1838.

(27) (a) Gans, P.; Sabatini, A.; Vacca, A. *Talanta* **1996**, *43*, 1739−1753. (b) Alderighi, L.; Gans, P.; Ienco, A.; Peters, D.; Sabatini, A.; Vacca, A. *Coord. Chem. Rev.* **1999**, *184*, 311−318.

(28) Deacon, G. B.; Phillips, R. J. *Coord. Chem. Rev.* **1980**, *33*, 227−250.

(29) (a) Sakiyama, H.; Tamaki, H.; Kodera, M.; Matsumoto, N.; Ōkawa, H. *J. Chem. Soc., Dalton Trans.* **1993**, 591−595. (b) Higuchi, C.; Sakiyama, H.; Ōkawa, H.; Isobe, R.; Fenton, D. E. *J. Chem. Soc., Dalton Trans.* **1994**, 1097−1103. (c) Higuchi, C.; Sakiyama, H.; Ōkawa, H.; Fenton, D. E. *J. Chem. Soc., Dalton Trans.* **1995**, 4015−4020.

(30) Sakiyama, H.; Sugawara, A.; Sakamoto, M.; Unoura, K.; Inoue, K.; Yamasaki, M. *Inorg. Chim. Acta* **2000**, *310*, 163−168.

(31) (a) Gultneh, Y.; Tesema, Y. T.; Yisgedu, T. B.; Butcher, R. J.; Wang, G.; Yee, G. T. *Inorg. Chem.* **2006**, *45*, 3023−3033. (b) Magnuson, A.; Liebisch, P.; Högblom, J.; Andurlund, M. F.; Lomoth, R.; Meyer-Klaucke, W.; Haumann, M.; Dau, H. *J. Inorg. Biochem.* **2006**, *100*, 1234−1243. (c) Gultneh, Y.; Tesema, Y. T.; Ahvazi, B.; Yisgedu, T. B.;

Butcher, R. J.; Tuchagues, J.-P. *Inorg. Chim. Acta* **2006**, *359*, 4463–4469.
(32) Sasaki, Y.; Akamatsu, T.; Tsuchiya, K.; Ohba, S.; Sakamoto, M.; Nishida, Y. *Polyhedron* **1998**, *17*, 235–242.
(33) (a) Dubois, L.; Xiang, D.-F.; Tan, X.-S.; Pécaut, J.; Jones, P.; Baudron, S.; Le Pape, L.; Latour, J.-M.; Baffert, C.; Chardon-Noblat, S.; Collomb, M.-N.; Deronzier, A. *Inorg. Chem.* **2003**, *42*, 750–760. (b) Blanchard, S.; Blain, G.; Revière, E.; Nierlich, M.; Blondin, G. *Chem. Eur. J.* **2003**, *9*, 4260–4268. (c) Blanchard, S.; Blondin, G.; Rivière, E.; Nierlich, M.; Girerd, J.-J. *Inorg. Chem.* **2003**, *42*, 4568–4578.
(34) Gultneh, Y.; Farooq, A.; Liu, S.; Karlin, K. D.; Zubeita, J. *Inorg. Chem.* **1992**, *31*, 3607–3611.
(35) (a) Hosssain, M. J.; Yamasaki, M.; Mikuriya, M.; Kuribayashi, A.; Sakiyama, H. *Inorg. Chem.* **2002**, *41*, 4058–4062. (b) Huang, C.; Xu, G.; Zhu, H.; Song, Y.; Gou, S. *Inorg. Chim. Acta* **2008**, *361*, 5–8.
(36) (a) Sakiyama, H.; Mochizuki, R.; Sugawara, A.; Sakamoto, M.; Nishida, Y.; Yamasaki, M. *J. Chem. Soc., Dalton Trans.* **1999**, 997–1000. (b) Erxleben, A.; Hermann, J. *Dalton Trans.* **2000**, 569–575. (c) Ye, B.-H.; Li, X.-Y.; Williams, I. D.; Chen, X.-M. *Inorg. Chem.* **2002**, *41*, 6426–6431.
(37) Kaminskaia, N. V.; Springler, B.; Lippard, S. J. *J. Am. Chem. Soc.* **2000**, *122*, 6411–6422.
(38) (a) Cotton, F. A.; Wilkinson, G.; Bochmann, M. *Advanced Inorganic Chemistry*, 6th ed.; Wiley: New York, 1999. (b) Dou, Y.-S. *J. Chem. Educ.* **1990**, *67*, 134–135. (c) Arora, H.; Lloret, F.; Mukherjee, R. *Inorg. Chem.* **2009**, *48*, 1158–1167.
(39) Singh, S.; Mishra, V.; Mukherjee, J.; Seethalekshmi, N.; Mukherjee, R. *Dalton Trans.* **2003**, 3392–3397.
(40) Mikuriya, M.; Fujii, T.; Tokii, T.; Kawamori, A. *Bull. Chem. Soc. Jpn.* **1993**, *66*, 1675–1686.
(41) Bu, X.-H.; Tong, M.-L.; Xie, Y.-B.; Li, J.-R.; Chang, H.-C.; Kitagawa, S.; Ribas, J. *Inorg. Chem.* **2005**, *44*, 9837–9846.
(42) Ménage, S.; Vitols, S. E.; Bergerat, P.; Codjovi, E.; Kahn, O.; Girerd, J.-J.; Guillot, M.; Solans, X.; Calvet, T. *Inorg. Chem.* **1991**, *30*, 2666–2671.
(43) Carrasco, R.; Cano, J.; Mallah, T.; Jones, L. F.; Collison, D.; Brechin, E. K. *Inorg. Chem.* **2004**, *43*, 5410–5415.
(44) (a) Rodriguez-Fortea, A.; Alemany, P.; Alvarez, S.; Ruiz, E. *Chem. Eur. J.* **2001**, *7*, 627–637. (b) Cano, J.; De Munno, G.; Sanz, J.; Ruiz, R.; Lloret, F.; Faus, J.; Julve, M. *J. Chem. Soc., Dalton Trans.* **1994**, 3465–3469.
(45) (a) Ruiz, E.; Alemany, P.; Alvarez, S.; Cano, J. *J. Am. Chem. Soc.* **1997**, *119*, 1297–1303. (b) De Munno, G.; Julve, M.; Lloret, F.; Faus, J.; Verdaguer, M.; Caneschi, A. *Inorg. Chem.* **1995**, *34*, 157–165. (c) Castro, I.; Julve, M.; De Munno, G.; Bruno, G.; Real, J. A.; Lloret, F.; Faus, J. *J. Chem. Soc., Dalton Trans.* **1992**, 1739–1744. (d) Delgado, F. S.; Sanchiz, J.; Lopez, T.; Lloret, F.; Julve, M.; Ruiz-Pérez, C. *CrystEngComm* **2010**, *12*, 2711–2721.
(46) (a) Kahn, O. *Molecular Magnetism*; VCH: New York, 1993. (b) Nishida, Y.; Kida, S. *J. Chem. Soc., Dalton Trans.* **1986**, 2633–2640.
(47) (a) Armentano, D.; Marino, N.; Martinez-Lillo, J.; Mastropietro, T. F.; Cano, J.; Julve, M.; Lloret, F.; De Munno, G. *Inorg. Chem.* **2008**, *47*, 10229–10231. (b) Tudor, V.; Kravtsov, V. Ch.; Julve, M.; Lloret, F.; Simonov, Y. A.; Averkiev, B. B.; Andruh, M. *Inorg. Chim. Acta* **2005**, *358*, 2066–2072. (c) Thompson, L. K.; Tandon, S. S.; Lloret, F.; Cano, J.; Julve, M. *Inorg. Chem.* **1997**, *36*, 3301–3306.
(48) (a) Figgis, B. N.; Gerloch, M.; Lewis, J.; Mabbs, F. E.; Web, G. A. *J. Chem. Soc. A* **1968**, 2086–2093. (b) Lines, M. E. *Phys. Rev.* **1963**, *131*, 546–555.
(49) (a) Herrera, J. M.; Bleuzen, A.; Dromzée, Y.; Julve, M.; Lloret, F.; Verdaguer, M. *Inorg. Chem.* **2003**, *42*, 7052–7059. (b) Lloret, F.; Julve, M.; Cano, J.; Ruiz-Garcia, R.; Pardo, E. *Inorg. Chim. Acta* **2008**, *361*, 3432–3445.
(50) (a) Cangussu, D.; Pardo, E.; Dul, M. C.; Lescouëzec, R.; Herson, P.; Journaux, Y.; Pedroso, E. F.; Pereira, C. L. M.; Stumpf, H. O.; Muñoz, M. C.; Ruiz-Garcia, R.; Cano, J.; Julve, M.; Lloret, F. *Inorg. Chim. Acta* **2008**, *361*, 3394–3402. (b) Tudor, V.; Marin, G.; Lloret, F.; Kravtsov, V. Ch.; Simonov, Y. A.; Julve, M.; Andruh, M. *Inorg. Chim. Acta* **2008**, *361*, 3446–3452.
(51) Mishra, V.; Lloret, F.; Mukherjee, R. *Inorg. Chim. Acta* **2006**, *359*, 4053–4062.
(52) Cano, J. *VPMAG*; Universitat de València, València, Spain, 2001.
(53) Mukherjee, A.; Lloret, F.; Mukherjee, R. *Eur. J. Inorg. Chem.* **2010**, 1032–1042.
(54) We admit that the kinetic data presented in this work are not of good quality (pseudo-first-order plots of a representative complex **2a** for the hydrolysis of HPNP are given in Figure S16 (Supporting Information); complexes **3a** and **4a** behave in a similar manner). Such plots are an indication that there is either an operational or mechanistic problem (the production of nitrophenolate ion/nitrophenol is not occurring in a "strict" first-order manner). Unfortunately, given the constraints of experimental conditions (buffer CHES (pH 8.50), $I$ = 0.1 M ($NaNO_3$) in MeOH/$H_2O$ (33%, v/v) at 30 °C), we are not in a position to obtain kinetic data that are any better than those obtained for the present study, as they are the best we could have. We are also convinced that no amount of analysis can improve the quality. However, the kinetic results—the relative trends—presented here convincingly demonstrate the effect of the bivalent metal ion in the hydrolysis/transesterification of HPNP for the chosen group of complexes. Given ESI-MS+ spectral analyses with excess substrate concentration (under the conditions of our measurement: MeOH/$H_2O$ (33%, v/v) at pH 8.5; complex/HPNP = 1/30), Figures S17–S19 (Supporting Information); see below), we rule out the possibility that the complexes **1a** (reported earlier) and **2a**–**4a** do not maintain their integrity during the reaction and are falling apart.
(55) Acharya, S.; Foldesi, A.; Chattopadhyaya, J. *J. Org. Chem.* **2003**, *68*, 1906–1910.
(56) Kolthoff, I. M.; Kameda, T. *J. Am. Chem. Soc.* **1931**, *53*, 832–842.